Available online at www.sciencedirect.com
SCIENCE DIRECT
Journal of Catalysis 230 (2005) 440–463
JOURNAL OF CATALYSIS
www.elsevier.com/locate/jcat

Embedded cluster (QM/MM) investigation of C6 diene cyclization in HZSM-5

Yogesh V. Joshi, Kendall T. Thomson *

School of Chemical Engineering, Purdue University, West Lafayette, IN 47907, USA

Received 16 September 2004; revised 10 December 2004; accepted 16 December 2004

Abstract

We preformed hybrid, embedded cluster calculations at the DFT/MM level to investigate cyclization of C6 diene leading to C6 cyclic product in HZSM-5. We observe that C6 diene cyclization can occur either directly from a physisorbed olefin or by first chemisorption to form an alkoxide intermediate. Furthermore, chemisorption can occur through a double-site mechanism or a single-site mechanism. We also observe two alternative pathways for cyclization starting from chemisorbed alkoxides. Primary alkoxides preferred direct 1,6 ring closure (17.7 kcal/mol activation energy), whereas secondary alkoxides only proceeded through a 1,5 ring closure to methylcyclopentene alkoxide (22.12 kcal/mol activation energy), followed by ring expansion through a stable bicyclo[3.1.0]hexane intermediate (21.31 kcal/mol activation energy for the rate-limiting step). Thus our calculations confirm that C6 dienes are likely to be the precursors for cyclization reactions. Finally, we show that embedded cluster calculations are essential for proper analysis of C6 olefin chemistry in ZSM-5 models—with fairly important distinctions between embedded cluster and bare cluster results.

Keywords: Aromatization; Cyclization; Zeolite; HZSM-5; Brønsted acid site; QM/MM ONIOM method; DFT; Embedded cluster model

1. Introduction

Direct conversion of light alkanes into aromatics with the use of MFI-based catalyst presents an economically attractive way of upgrading light feedstocks like liquefied petroleum gas (LPG) [1–3]. The products contain a significant fraction of aromatics, particularly benzene, toluene, and xylenes (BTX), used in different downstream petrochemical processes. Medium-pore zeolites like ZSM-5 provide an efficient way to control the product distribution because of their shape-selective catalytic properties [4–8]. However, substantial cracking activity of the Brønsted acid sites in HZSM-5 limits the aromatics selectivity. The rate-limiting steps of the initial olefin generation are overcome by the addition of dehydrogenation activity to the catalyst. This dehydrogenation function prevents redistribution of the hydrogen and generates molecular hydrogen as a valuable side product. Extraframework species like Ga [9–15], Zn [16–20], and Pt [21–26] have been commercially used for this purpose. However, with added dehydrogenation activity, these catalysts suffer from the major drawback of faster deactivation.

In light of these facts, significant efforts have been made in catalysis research to develop a highly selective aromatization catalyst with reduced deactivation rates. Even with single-component feedstocks like propane, this problem is very complicated. It involves a complex reaction network with scores of intermediates. This reaction network for propane aromatization on HZSM-5 is summarized in Scheme 1 [4] and involves reaction families like (1) alkane C–H activation, (2) dehydrogenation to olefins, (3) protolytic cracking, (4) oligomerization to higher olefins, (5) isomerization, (6) β-scission, (7) cyclization, and (8) dehydrogenative aromatization [27]. Because of the interconnectedness of this reaction network, it is very difficult to decouple any reaction family and study it separately with regular experimental setups. Most of these reaction

* Corresponding author. Fax: (765) 494-0805.
E-mail address: thomsonk@purdue.edu (K.T. Thomson).

0021-9517/$ – see front matter
doi:10.1016/j.jcat.2004.12.016

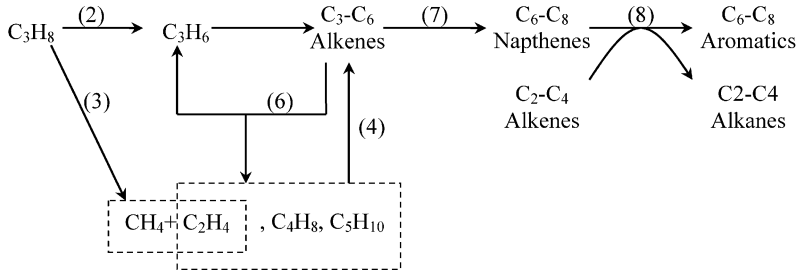

Scheme 1. Reaction pathways [4] for propane aromatization using HZSM-5.

paths are based on superacid catalyzed reactions derived from carbenium/carbonium ion chemistry [28]. However, a detailed understanding of each reaction step is necessary for the preparation of a kinetic model of sufficient complexity. Current understanding of each reaction step is based on the experiments under special conditions involving lower temperatures and pressures, limiting the conversion of the various feed molecules. For example, initial activation of the propane was studied at very low conversion to draw conclusions about reaction orders for cracking [29]. Similar methods were used to study monomolecular conversions, cracking vs dehydrogenation for light alkanes [30,31].

Based on the role of the catalyst, cyclization reaction can be classified into three categories:

(1) *Cyclization in the presence of metal oxides like Ga_2O_3 or ZnO_3*. According to this mechanism C6+ hydrocarbons undergo catalytic dehydrogenation over sites on the oxide phase to form trienes, which then undergo nonionic gas-phase thermal pericyclic reactions to form cyclohexadiene. This mechanism was studied experimentally [26,32,33] with the use of *model reactants* like propane, hexane, heptane, propene, 1-hexene, cyclohexane, cyclohexene, and methylcyclopentane. According to these studies paraffins and saturated naphthenes (e.g., cyclohexane, methylcyclohexane) do not undergo dehydrogenation. However, there are significant differences in the activity of Ga_2O_3 toward aromatization. It was shown [34] that Te–NaX is very active and selective for the aromatization of *n*-hexane. Isotopic labeling studies [35] showed that this catalyst operates via the above-mentioned cyclization mechanism.

(2) *Cyclization catalyzed by supported noble metals like Pt on Al_2O_3, Pt-HZSM-5*. In the case of acidic supports, the bifunctional route is preferred. The actual cyclization step is catalyzed by acid centers on the support. Cyclization by both 1,5 and 1,6 ring closure has been hypothesized in these cases. For Pt on nonacidic supports, a monofunctional mechanism has been proposed. Here it has been postulated that 1,6 ring closure dominates over 1,5 ring closure [26].

(3) *Cyclization catalyzed by Brønsted acid sites in the zeolite*. Considering the strong acidity of the Brønsted acid sites in the zeolite, a mechanism based on carbenium ion chemistry has been suggested. Several experimental investigations using model reactants [6,26,36] have led to important conclusions, namely that (i) dienes or trienes are the precursor for cyclization, (ii) naphthenes like cyclohexane are unlikely to be the intermediates for cyclization on monofunctional Brønsted acid zeolites, and (iii) ring closure to cyclic olefins is irreversible. These studies concluded that ring closure is less activated than other important reactions like dehydrogenation and cracking. Despite this fact, the study of cyclization is essential, considering its direct influence on the product distribution of the aromatics.

The well-accepted alkoxide nature of the reaction intermediates involved in cyclization limits the extent to which gas-phase carbocation chemistry can guide our intuition and understanding. Thus our intention in this work is to extend our previous density functional theory (DFT) study of gas-phase cyclization [37] by taking into account the active site as well as the ZSM-5 microstructure. Ab initio density functional theory (DFT) has been extensively used to study reaction steps like olefin chemisorption [38–41], protolytic cracking [42–44], beta-scission [45,46], hydride transfer [47,48], and dehydrogenation [49,50]—all based on alkoxide-like intermediates. However, the study of Brønsted acid-catalyzed cyclization with molecular simulation methods is unprecedented to the authors' knowledge.

In our previous work [37] we studied gas-phase cyclization of carbenium ions generated by protonation of the hexadiene. In the gas phase, we identified two reaction paths leading to the cyclic product. Cyclization could proceed via methylcyclopenta carbenium ion as per the classical carbenium ion mechanism (as shown in Scheme 2a). In addition, there is a possibility of direct cyclization via 1–6 ring closure (as shown in Scheme 2b). In superacid media, stable carbenium ions are observed experimentally [28]. However, it has been shown, both experimentally [51] and by ab initio simulations [38], that the stable intermediates resulting from olefin chemisorption form covalent bonds with the conjugate base (deprotonated Brønsted acid site), resembling alkoxides rather than free carbenium ions. We subsequently expect cyclization to proceed through alkoxide intermediates near Brønsted sites. Interestingly, the transition states involved in this chemistry are more cationic in nature, resembling carbenium ion species. Hence, the stability of transition states and

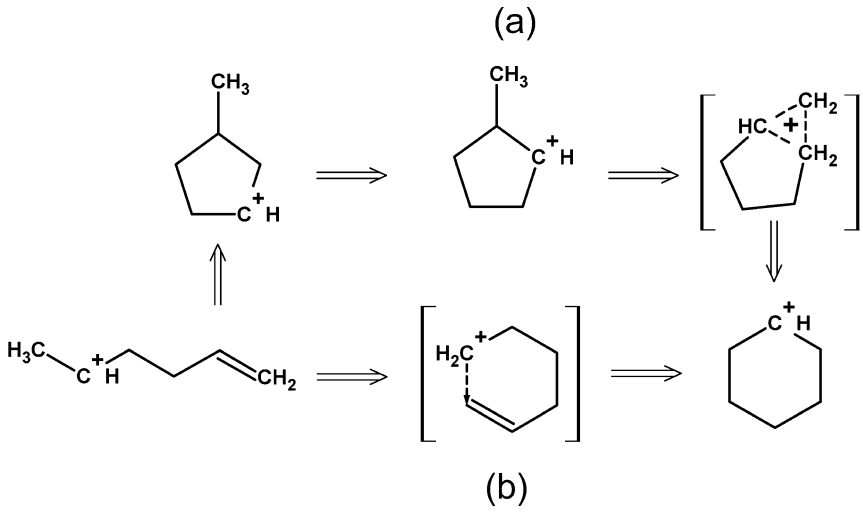

Scheme 2. Two reaction paths for gas phase cyclization of the protonated diene.

therefore activation energies are directly analogous to carbocation stability, which is useful in the analysis of viable pathways.

In this work we used hybrid molecular simulation methods to study the cyclization reaction step catalyzed by the Brønsted acid site in HZSM-5. In particular, we used electronic density functional theory (DFT) combined with molecular mechanics to study various cyclization paths for C6 dienes. We have performed these calculations with the use of two different levels of theory: (1) pure DFT cluster calculations, and (2) hybrid (QM/MM) methods. The pure DFT calculations involved a cluster with 11T positions from the zeolite lattice. However, these cluster models do not adequately capture the extended pore structure, omitting the entire pore wall surrounding the site. Hence confinement effects, which we anticipate are essential for quantifying aromatics selectivity, are not adequately modeled. We correct for this by extending the pure DFT calculation in a QM/MM hybrid calculation that models the full pore structure at the molecular mechanics level.

The rest of this paper is organized as follows. In Section 2 we describe the computational details of our calculations. Section 3 consists of the results and discussions of our calculations, including our analysis of detailed reaction pathways containing energetics for both 1,6 ring closure and 1,5 ring closure followed by ring expansion of hexadiene. In Section 4 we summarize the important conclusions of our work.

2. Cluster model and details of the calculations

In all of this work, we employed the finite cluster approximation for our catalyst site model. Since we are dealing with large hydrocarbon molecules, a sufficiently large cluster is needed to model any sort of shape selectivity. Such a large cluster would be impractical for the intended level of theory. To overcome this problem we employ embedded cluster models [52,53]. As a result, most of the calculations were performed with two types of clusters (structure I in Fig. 1). One of the two clusters (Fig. 1a) is built around the T12 site of ZSM-5 with a total of 11 T sites in the cluster. The geometry of this cluster is prepared from the ZSM-5 crystal lattice structure reported in the literature [54].

The T12 site is located at the cross section of the straight channel and sinusoidal channel; hence, it is believed to be one of the more active sites in ZSM-5, being the most accessible and offering the largest space in the pore structure for hydrocarbon transformations. A recent ion pair shell model simulation of the Brønsted acid location in the MFI framework [55] indicated a very narrow energy distribution (2–3 kcal/mol) of these sites. Hence, although other T sites like the T7 site are also valid options, we chose the T12 site because it is likely to be the most accessible for large hydrocarbons. From this point we refer to this 11 T cluster as the *bare cluster* (BC). The 11 T bare cluster is terminated with the use of Si–H groups with a Si–H bond length of 1.4979 Å. Si and H from terminal groups are maintained at fixed Cartesian positions throughout the calculations. A 6-31g(d,p) basis set was used for all of the calculations with the B3LYP hybrid density functional [56].

The second cluster represents an *embedded cluster model*. It consists of two layers, as shown in Fig. 1b. The innermost layer consists of the 11 T sites and hydrocarbon species. These 11 T sites are the same T-sites from the bare cluster calculations. The outer layer consists of 127 T sites located symmetrically around an inner 11 T cluster. Thus, in total, the embedded cluster (EC) consists of 138 T sites. It has been shown [57] that one achieves a convergence with respect to long-range van der Waals interactions for such a size of the cluster. This cluster represents the complete intersection of the straight channel and sinusoidal channel, which is important in accounting for the shape-selective effects of the zeolite cavities. The outer layer of the embedded cluster is terminated with fixed Si–H bonds with a Si–H distance fixed at 1.47 Å. Si–H distances were decided according to the level of the theory relevant for the respective

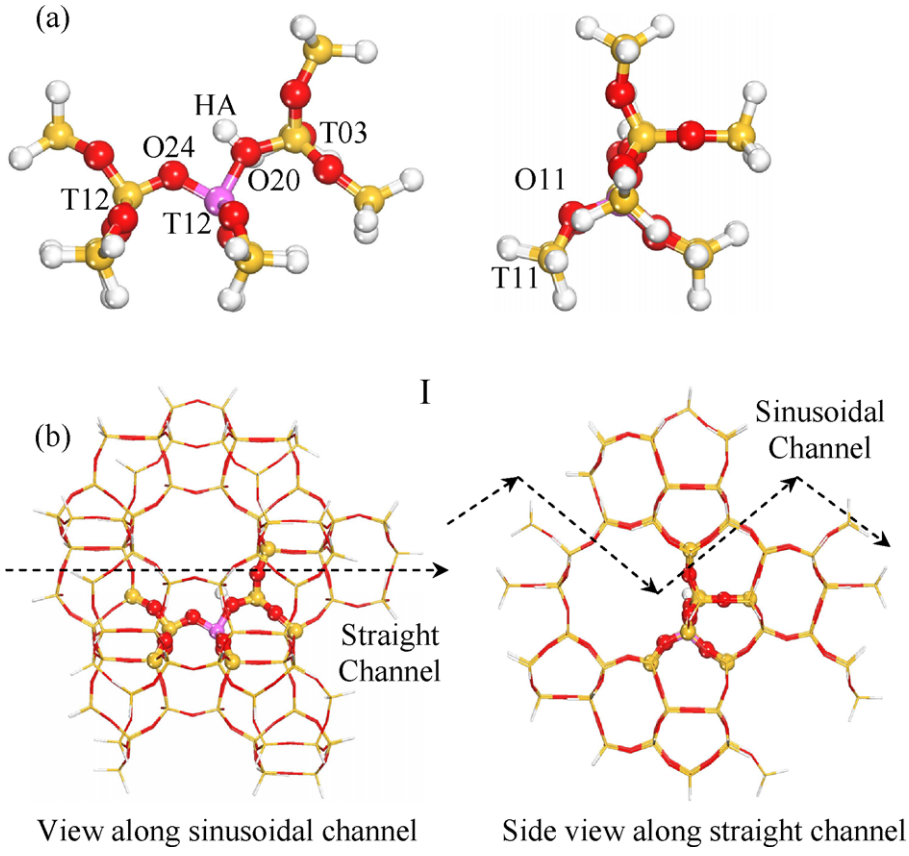

Fig. 1. Zeolite clusters for T12 Brønsted acid site (I) from MFI framework, (a) bare cluster (BC) with 11 T sites; (b) embedded cluster (EC) with total 138 T sites.

layer. This consideration was important for QM since it has been observed [58] that the Si–H bond lengths directly affect the acidity of the Brønsted sites. Embedded cluster calculations were implemented according to the two-layer ONIOM methodology [59]. The higher-level calculations were done with the use of the 6-31g(d,p) basis set and B3LYP hybrid functional [56] as before. Molecular mechanics and the universal force field (UFF) [60] were employed as a lower-level theory. The UFF atom types for Si, O, and Al were specified as Si3, O_3_z, and Al3, respectively [60]. All of our calculations were done with the Gaussian 03 program package [61].

The main purposes of these embedded cluster calculations are (1) to simulate the geometry constraint due to the zeolite channel structure at the smallest computational cost and (2) to account for the long-range attraction due to dispersion forces. With these objectives in mind, certain assumptions were made. We fixed all of the atoms in the outer layer to their respective crystallographic positions, with the idea that this speeds up geometry convergence and at the same time reduces the possibility of the error due to less accurate force-field parameters.

To investigate the accuracy of the UFF, we compared disiloxane ($H_3Si–O–SiH_3$) geometry for UFF and DFT. A similar comparison was made by Sierka et al. [62] to validate the ion-pair shell potentials for zeolite. We found that UFF underpredicts the Si–O bond length by 0.05 Å. Thus relaxation of the outer layer treated exclusively by UFF would lead to unnatural geometry of the strained cluster. Thus to draw a reliable comparison between the bare cluster and embedded cluster results, we have constrained the atoms from the outer layer. However, as shown by Rozanska et al. [63], relaxation of the nearest-neighbor T sites along with all of the bridging oxygens is necessary if we are to draw quantitative conclusions. Hence, we allowed full relaxation of all QM atoms in our QM/MM model, including the 10 T sites around the Al at the T12 position (including four nearest neighbors) and the bridging oxygens.

To test our approximation of freezing MM-level coordinates, we conducted several calculations to try and quantify the effects of MM-level relaxation. In particular, we compared the QM/MM energy of reaction for cyclization via 1,6 ring closure (a key reaction in our study) before and after relaxation of the atoms upto all third nearest-neighbor T sites of the Al at T12. We observe that the energy of reaction (VI $\rightarrow$ TS_3 $\rightarrow$ VIII) shifted by $\sim$ 4.6 kcal/mol (from -13.67 to -18.28 kcal/mol), and the activation energy changed from 17.69 kcal/mol (before MM atoms relaxed) to 19.58 kcal/mol (after relaxation). Even though there is fairly large stabilization of each geometry optimization due to MM-level relaxation, the effects on energy differences cancel out and do not appear to be drastic. Since it

is known that force-field models like UFF are not accurate for simulating zeolite structures, we believe that *relaxation* of the outer MM layer would lead to more uncertainty than the correction of any approximation involved.

Recently there have been several investigations [44,52,64,65] regarding the importance of the electrostatic field in molecular simulations of this system. The effect of long-range electrostatic forces can be accounted for by either electronic or mechanical embedding. In electronic embedding the point charges [66,67] are used to simulate the electrostatic field around the active site, thus directly polarizing the QM part of the calculations. However, the electronic embedding is very sensitive to the treatment of the point charges at the boundary between the QM and MM atoms. Sinclair et al. [68] reported higher ΔE of formation for the stable isobutyl carbenium ion after inclusion of the electronic and MM embedding. This observation was attributed to the shape-selective effect of the chabazite framework, as the electronic embedding is expected to stabilize the carbocationic species. In mechanical embedding the point charges are not explicitly included in the QM calculations, whereas a correction term based on the force-field models is added in the QM energy.

The advantage and reliability of the classical embedding are demonstrated by Sauer et al. by calculation of NH_3 adsorption in faujasite [69] and proton mobility [70]. A similar hybrid method used by Boronat et al. [41] used a semi-empirical MNDO as the lower-level theory to find a structure-activity relation for alkene chemisorption. Some of these studies [41,44] conclude that the short- to medium-range part of the Madelung potential is effective in the stabilization of the ionic transition states.

Another approach by Tuma et al. [71], involving MP2/planewave-DFT, simultaneously accounts for electrostatic interactions and corrects the DFT calculation with a post-Hartree–Fock method like MP2. Sauer et al. [52] have demonstrated convergence for proton jump barriers with the use of an 8T cluster along with classical treatment of the polarization in the QM/MM model.

A recent study by Boronat et al. [41] points out that *the short-range part of the electrostatic field* is important for the stabilizations of the carbocationic TS. Hence, since the carbocationic transition states are necessarily associated strongly with the catalytic site, having a large enough QM cluster should be adequate to capture the important local electrostatics interactions reasonably well. In our investigation, we found that total energies were very sensitive to the partial charge values and how the charge equalization (qeq) is conducted. Furthermore, most of the reaction pathways we investigated involved transitions from alkoxides to carbocation-like transitions states, with significant differences in charge distribution among these conformations. Without an accurate procedure to account for these charge differences, we believe the use of *force-field-derived* partial charges in our calculations would have been more artificial than not including them.

Table 1
Comparison of the Brønsted acid site geometry for bare cluster and embedded cluster calculations

Geometry parameter	Bare cluster	Embedded cluster
O20–HA (Å)	0.971	0.971
T12–O20 (Å)	1.845	1.840
T12–O24 (Å)	1.700	1.691
T12–O20–T03 (deg)	135.11	135.06
T12–O24–T12 (deg)	123.75	122.35
T12–O11–T11 (deg)	135.0	147.7

To test this, we compared the energetics with and without qeq charges [60] for key reaction steps discussed in this contribution—including qeq charges in conjunction with UFF. As qeq charges depend on the geometry, we expect them to change with geometry optimization. However, most of the molecular simulation packages (for example, Gaussian 03) do not implement this feature, since it can adversely affect the robustness of geometry optimization algorithms. To overcome this problem we iterated manually through the geometry optimization process, updating the partial charges at each new geometry, to achieve convergence with respect to energies and charges corresponding to the optimal geometry. This procedure is essential for the proper incorporation of qeq charges, in that the total energies are very sensitive to the qeq charges (which depend on geometry). For both 1,6 and 1,5 ring closure steps, we found that the activation energy uniformly increased by roughly 4–5 kcal/mol. Thus we conclude that with a large enough QM-level cluster, partial charges in the MM level result in a roughly constant shift in activation energies, and not necessarily in a stabilizing manner. In our model, the important carbocation stabilizing effects are inherently included in our QM level (like polarization of C–H bonds). Furthermore, we conclude that comparisons between activation energies of competing pathways are reasonably quantitative.

For rest of the QM/MM results, we have not used the partial charges on the atoms in conjunction with the UFF. As a consequence, our embedded cluster results do not reflect the explicit charge embedding of the inner QM layer. In Table 1 we show a comparison between bare cluster and embedded cluster geometries. As expected, the differences in the active site geometries are minimal. In all reported energetics, we neglect basis set superposition error (BSSE) and zero-point energy correction.

Transition states are calculated with the quadratic synchronous transit (QST) method [72]. The validity of the critical transition states is confirmed with the use of (1) imaginary frequency mode visualization, (2) relaxation by perturbing transition states along the imaginary frequency modes, and (3) rigorous internal reaction coordinate (IRC) [73] relaxation. For brevity we will denote bare cluster results by “BC” as a prefix and embedded cluster results by “EC” as a prefix.

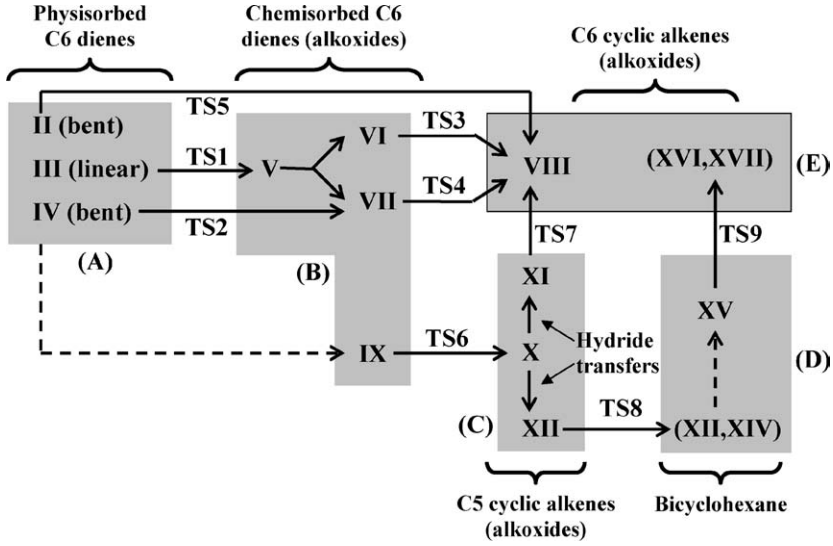

Scheme 3. Summarized reaction network for cyclization of 1,5 hexadiene catalyzed by HZSM-5.

3. Results and discussion

Scheme 3 shows a summarized representation of the intermediates and pathways we investigated. Ring expansion, 1,6 cyclization, and 1,5 cyclization are discussed separately in the following subsections.

3.1. 1,6 cyclization of C6 diene

In this work we identify two pathways for 1,6 ring closure for 1,5-hexadiene. The first reaction path is a two-step process starting from a physisorbed hexadiene molecule. Our gas-phase cyclization study [37] clearly demonstrates the possibility of several conformers for acyclic intermediates. These conformers can be broadly categorized as bent conformers or linear conformers. In addition, there are several alternatives for modeling the Brønsted proton, which can be present on different oxygens surrounding the T12 site. Hexadiene can physisorb at T12–O20–T03, as a bent conformer (II) or as a linear conformer (III). Hexadiene can also physisorb at the Brønsted site comprising the T12–O11–T11 bridge, represented as the bent conformer IV shown in Fig. 2e. Embedded cluster physisorption energies for structures II and III are 28.43 and 28.67 kcal/mol, respectively (BC energies 8.22 and 7.83 kcal/mol). For structure IV, physisorption energies are 30.50 and 6.46 kcal/mol for EC and BC, respectively. As expected, there is a significant contribution of the van der Waals forces to the physisorption energies. As shown previously in the literature [57], embedded cluster calculations accurately represent the hydrocarbon physisorption process inside zeolite channels. In subsequent energy diagrams reporting both BC and EC reaction paths, we assume the EC energies as our reference and shift all BC energies such that the physisorbed states of III are equal. Thus the physisorbed states of alkenes are aligned at same energy level for EC and BC calculations. This shift in the potential energy surface provides a common reference energy for direct comparison between the EC and BC potential energy surfaces. The zero energy of all potential energy diagrams corresponds to the sum of the total energy of the linear 1,5-hexadiene (outside zeolite cavity and at infinite distance) and the EC Brønsted acid site at the T12–O20–T11 bridge position.

The chemisorption of the various physisorbed hexadienes to form alkoxide is shown in Scheme 3 by arrows between block A (physisorbed species) and block B (chemisorbed alkoxides). Of the three physisorbed structures, IV can undergo protonation at the secondary carbon (C2) and chemisorption to primary alkoxide at C1 to give the bent chemisorbed conformer VII. This classical mechanism for chemisorption needs two bridge oxygen sites from the conjugate base along the zeolite wall. One of the bridge oxygens (T12–O11–T11) donates the Brønsted proton to the secondary (β) carbon, and the other bridge oxygen (T12–O20–T03) forms an alkoxide-like bond with the primary (α) carbon. Thus, a necessary condition for this two-centered reaction path is that the hydrocarbon should be oriented in such a way that two carbon atoms from C=C can easily interact with the two oxygen sites. The activation barrier we calculated for this "double-site" pathway with the use of the EC model was 25.35 kcal/mol. For the BC model the same pathway resulted in an activation barrier of 23.98 kcal/mol.

However, for the physisorbed intermediates II and III, such pathways are not feasible since the above-mentioned conditions are not satisfied. Both carbons from C1=C2 have only O20 in proximity. Hence we computed a mechanism involving protonation and chemisorption involving the same T12–O20–T03 bridge site. This type of "single-site" mechanism for propene chemisorption is described in our previous publication [40]. We show that the linear physisorbed 1,5-hexadiene (II) undergoes protonation to form a chemisorbed primary alkoxide intermediate by the single-site pathway. As shown in Fig. 3, the reaction pathway for chemisorp-

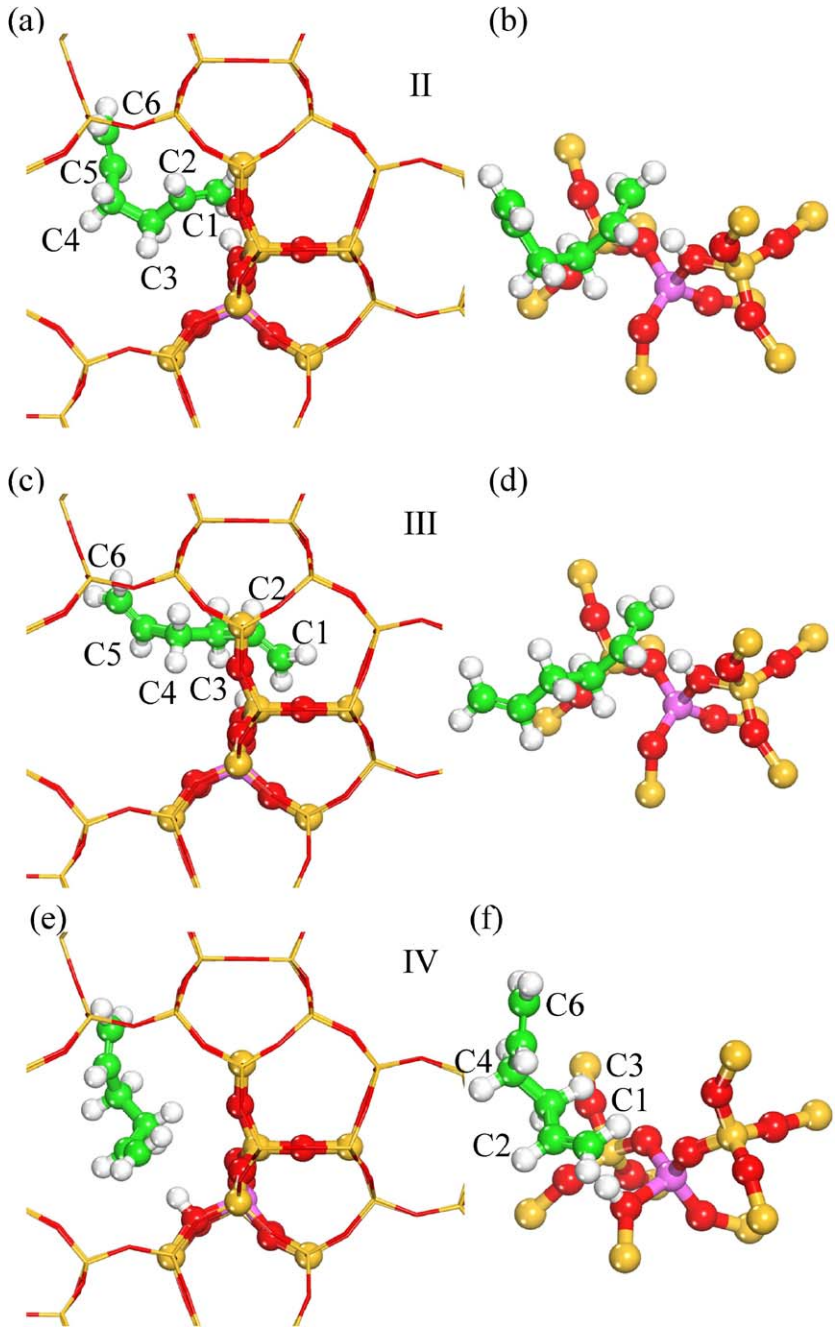

Fig. 2. Different conformers for the physisorbed 1,5-hexadiene, (a) bent conformer and (c) linear conformer physisorbed on Brønsted site at T12–O20–T03; (b) and (d) bare cluster analogue of (a) and (b); (e) bent physisorbed conformer on Brønsted site at T12–O11–T11; (f) bare cluster analogue of (e).

tion of the linear hexadiene resulted in an activation barrier of 36.02 kcal/mol for the EC model. Since the double-site pathway involves two charge centers and the single-site mechanism requires only one charge center, the activation barrier for the single-site mechanism is higher than the two-site mechanism.

The EC calculated transition state geometry (TS_1 shown in Fig. 4) indicates that the tail of the C6 chain is forced to align along the sinusoidal channel, whereas in the BC, we were unable to find a transition state for the single-site chemisorption pathway. The reason for this is that in the absence of the extended zeolite structure constraint, the less constrained hydrocarbon tail reorients such that the final transition state represents a completely different (not reported) reaction path. This result signifies the importance of the extended zeolite framework for the study of reactions involving longer hydrocarbons. Protonation of the bent conformer (III) leads to a surprisingly different reaction path that is described later in this subsection.

The resulting linear chemisorbed intermediate (V) can structurally reconfigure to either of two bent conformers (VI or VII) by simple dihedral rotations. Activation bar-

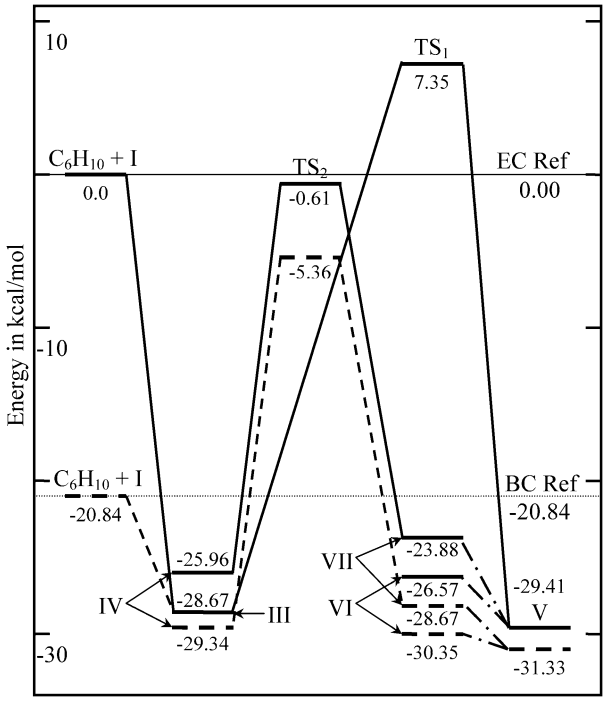

Fig. 3. Reaction path (network) for adsorption of 1,5-hexadiene as primary alkoxide on T12–O20–T03 site. C_6H_{10} linear 1,5-hexadiene; III—linear hexadiene physisorbed on Ha–O20 Brønsted site; IV—bent hexadiene physisorbed on Ha–O11 Brønsted site; TS_1—transition state for single-site mechanism; TS_2—transition state for two-site mechanism; V—linear chemisorbed hexadiene; VI—bent (Chair) chemisorbed diene; VII—bent (boat) chemisorbed alkoxide. Solid line: embedded cluster and dashed line: bare cluster.

riers for these steps are expected to be small. After the physisorbed states are aligned on the potential energy surface, the difference between the EC and BC energies is a direct measure of the activation or deactivation due to geometry constraint of the zeolite pore. We notice that one of the bent conformers of the chemisorbed diene (VI) is 2.84 kcal/mol (BC: 0.98 kcal/mol) higher in energy with respect to the linear conformer, and the other (VII) is 5.53 kcal/mol (BC: 2.66 kcal/mol) higher with respect to the linear conformer (V). As expected, the bent conformer was more activated because of greater channel constraint compared with the linear chemisorbed species. Geometries for all three chemisorbed conformations are shown in Fig. 5.

Formation of the linear conformer (V) and rearrangement to either of the bent primary alkoxides (VI or VII) is followed by ring closure. This step, along with the intermediate species involved, is depicted in Scheme 3 by arrows between block B and block E (chemisorbed cyclic products). Reaction paths for ring closure via 1,6 ring closure are shown in Fig. 6. Cyclization is facilitated by an intramolecular nucleophilic attack of the electron-rich terminal carbon (C6) on the electrophilic alkoxide center at the C1 position. This leads to the formation of a covalent bond between C1 and C6. The reaction coordinate is predominantly described by an increasing C1–O20 distance and a decreasing C1–C6 distance. After ring closure the cationic center shifts from the C1 position to C5. We carried out geometry relaxation of the transition states by perturbing it along the reaction path (eigenvector corresponding to the single imaginary frequency). We confirmed (not reported) that the cyclic carbocation rotated and re-adsorbed on the adjacent oxygen (T12–O24–T12) from the conjugate Brønsted base. The total energy change for this ring closure step is −13.67 kcal/mol (BC: −16.08 kcal/mol) for conformation VI. Transition states for 1,6 ring closure were observed to have either a chair (TS_3) or boat (TS_4) conformation. Both of these geometries are shown in Fig. 7. For ring closure via the chair conformation, our EC calculation gives an activation barrier of 17.69 kcal/mol, and for the BC it is 18.46 kcal/mol. The boat conformation reaction path is activated by 17.72 kcal/mol (EC) and 18.87 kcal/mol (BC). As shown in Fig. 6, we find the boat conformer reaction path is more activated than the chair conformer. This seems logical, since during cyclization the chair conformer can maintain closer proximity with the active site compared with the boat conformer. The resulting re-adsorbed cyclohexene intermediate (VIII) is shown in Fig. 8. For the EC geometry the chemisorption energy of cyclohexene was −17.73 kcal/mol (BC: −3.08 kcal/mol).

We report the total Mulliken charge on the hydrocarbon fragment (defined as the sum of partial charges on nonzeolite atoms) and important geometry parameters for VI, VII, TS_3, TS_4, and VIII in Table 2. Transition state TS_3 exhibited a 0.74 fragment charge versus 0.46 for reactant (VI) and product (VIII). This clearly demonstrates the carbenium nature of the transition state compared with the alkoxide nature of the reactant or the product. For the EC model, the TS hydrocarbon fragment resides farther from the active site (conjugate base) compared with the BC model. However, the most interesting difference is the C1–C6 distance for the bent chemisorbed hexadiene intermediate. In the structure VI the C1–C6 distance for our BC calculation was 3.765 Å, whereas for the EC calculation it was 3.573 Å. Similarly for intermediate VII, the C1–C6 distance decreased from 3.344 Å (bare cluster) to 3.285 Å (embedded cluster). We also note that the EC cluster, relative to the BC cluster, elevates the energy of (activates) the bent conformers VI and VII more so than the linear chemisorbed conformer V—by 3.78 and 4.77 kcal/mol versus only 1.92 and 2.66 kcal/mol. Thus it is apparent that the extended zeolite channel provides stronger net activation for bent chemisorbed precursors during cyclization. This clearly indicates the shape-selective reactant activation by MFI pore structure to facilitate ring closure. However, the effect of the extended structure of the embedded cluster is very small on transition-state geometries TS_3 and TS_4 reported in Table 2. We notice for the bare cluster calculations that the C1–C6 distance decreases from VI to VII to TS_3 to TS_4. Since the C1–C6 distance is an indication of the size of the hydrocarbon species, it is expected that the larger alkane will show a larger change in the geometry (i.e., a larger decrease in the C1–C6 distance) in the embedded cluster calculation. The reported C1–C6 dis-

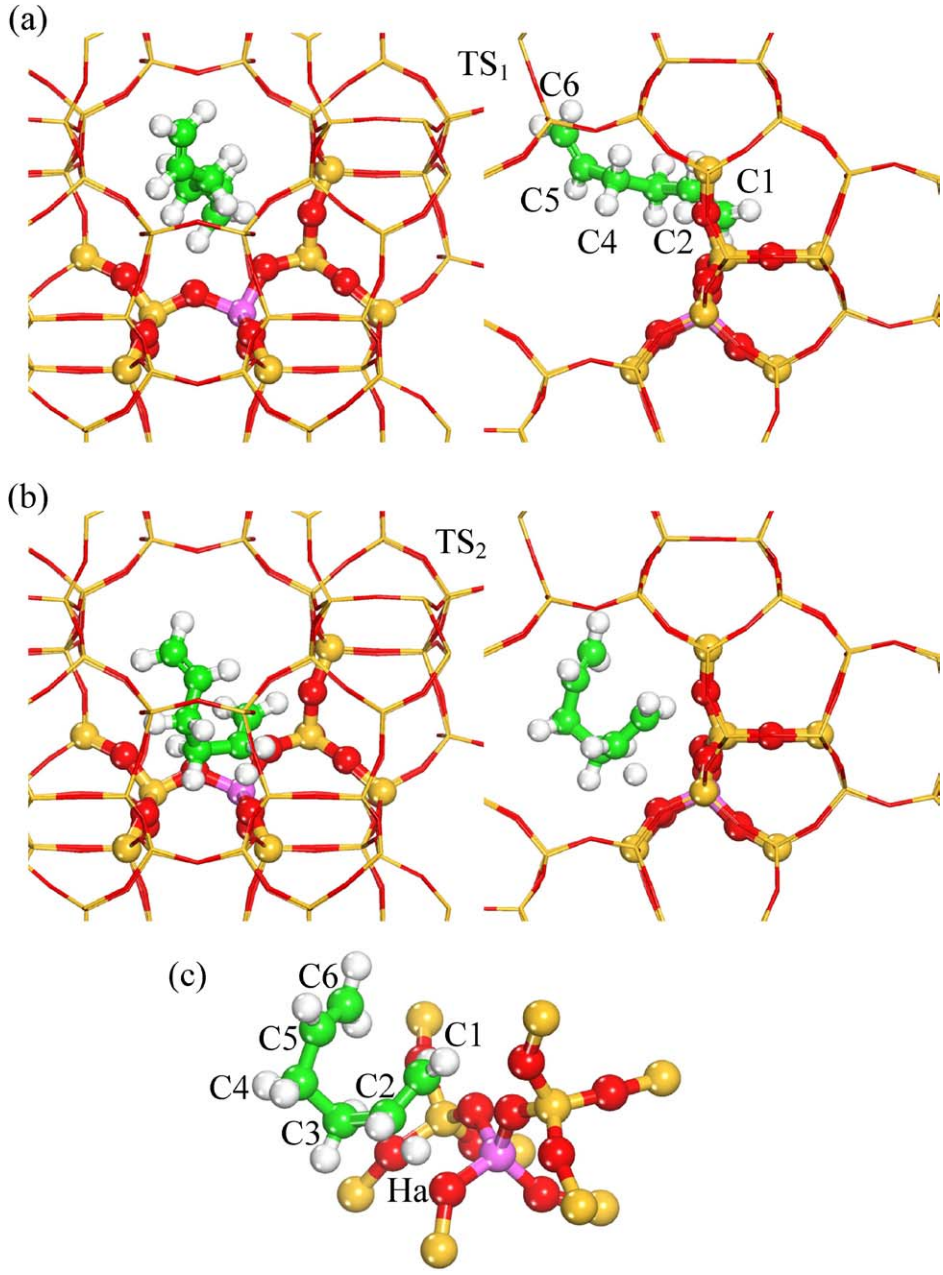

Fig. 4. Transition state for (a) chemisorption of a linear 1,5-hexadiene on Brønsted acid site constrained by extended zeolite structure: single-site mechanism involving only T12–O20–T03 bridge position; (b) chemisorption of the bent 1,5-hexadiene: two-site mechanism involving T12–O11–T11 and T12–O20–T20 bridge sites; (c) bare cluster analogue corresponding to (b).

tances in Table 2 confirm this speculation. Rigidity of the cyclic product could be another factor contributing to this trend.

The bent conformer (II) of the physisorbed diene is shown in Fig. 2a. For the reasons stated earlier in this subsection, the bent hexadiene physisorbed on the Brønsted acid (T12–O20–T03) site cannot follow a double-site chemisorption mechanism. Starting from this physisorbed species, there is a possibility of a simultaneous protonation and ring closure (skipping a chemisorbed state). In Scheme 3, this reaction is depicted by an arrow between the block A and block E. The reaction path and transition state for such a mechanism are shown in Fig. 9. Relevant geometry parameters are presented in Table 3. During protonation of C2 from the C1=C2 double bond, a significant positive charge on the primary carbon is developed. The charge on C1 increases by 0.296 au, going from reactant II to transition state TS_5. For the bent conformer, this active carbocationic center undergoes nucleophilic attack by the terminal C6 carbon. Thus after protonation, the proximity of the terminal carbon C6 and carbocationic center C1 obviates the chemisorption possibility seen in the case of the linear hexadiene (III). The activation

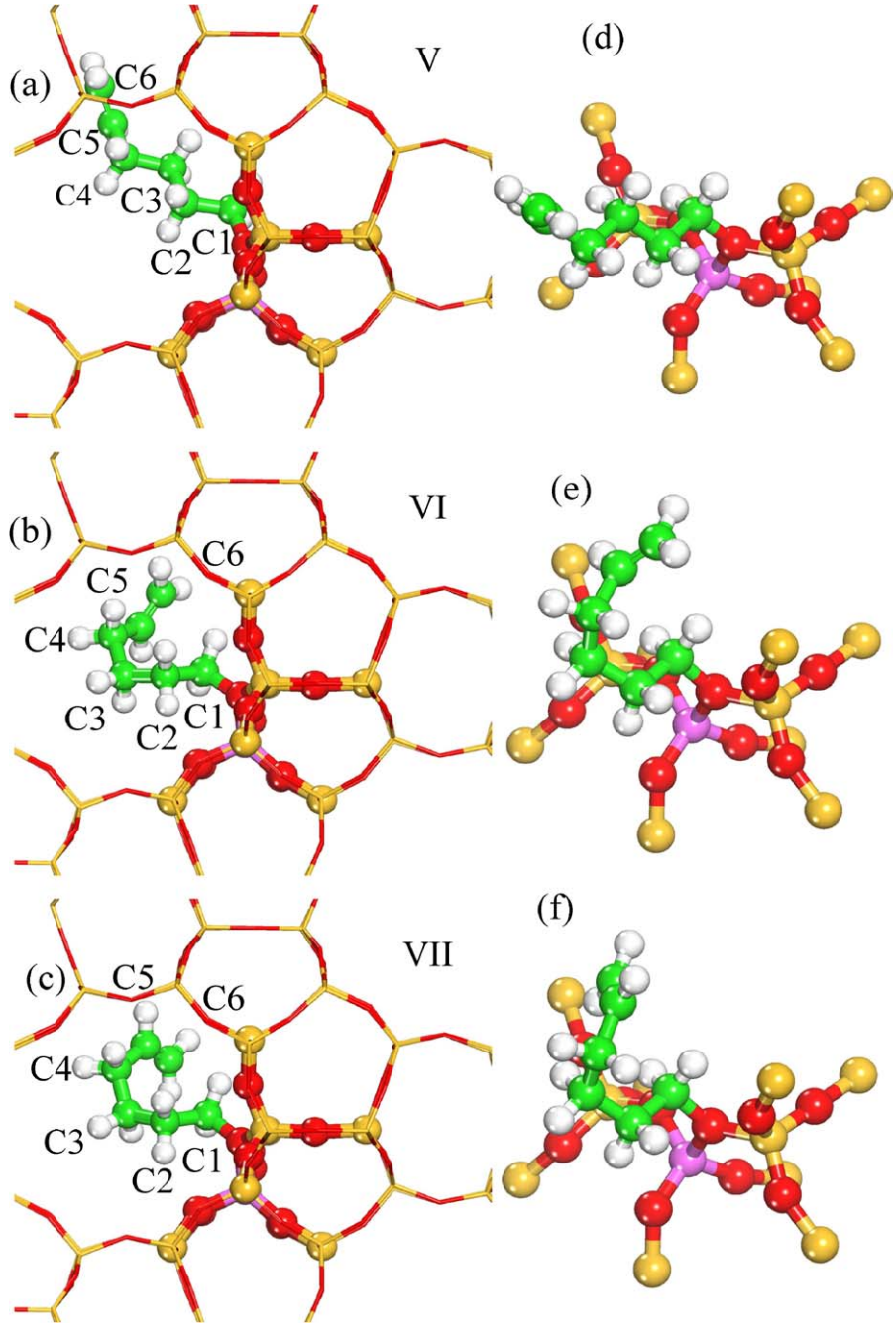

Fig. 5. Three conformers for the chemisorbed 1,5-hexadiene, (a) linear conformer as precursor for bent conformer; (b) bent conformer leading to TS_3 (chair) for 1,6 cyclization; (c) bent conformer leading to TS_4 (boat) for cyclization; (d); (e); and (f) bare cluster analogue of (a), (b) and (c), respectively.

barrier for such a cyclization path (TS_5), from bare cluster calculation, is 23.23 kcal/mol. For the embedded cluster calculation, it is 26.60 kcal/mol.

We note that the activation barriers for cyclization starting from chemisorbed species are less in EC calculations compared with BC calculations. However, for cyclization starting from physisorbed species, EC calculations give higher activation barriers with respect to BC calculations. It is clear that the van der Waals potential field due to the extended zeolite structure modifies the potential energy surface for hydrocarbon pathways. The extent of this modification is determined by the number of carbon atoms and their average distance from the zeolite walls.

In Fig. 10 we propose a simple explanation for this trend. We note that the effects of the van der Waals interactions in the EC calculations are virtually entirely attractive. However, for species located farther from the active site (and more toward the center of the channel intersection), the attractive contribution in the EC calculation is larger than for species closer to the site. In general one finds a physisorbed

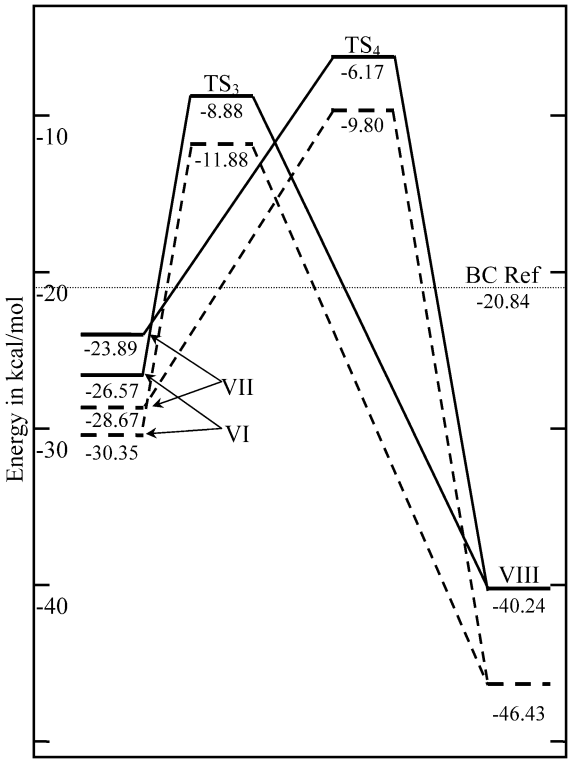

Fig. 6. Reaction path for 1,6 ring closure of primary alkoxide (chemisorbed 1,5-hexadiene), VI and VII—bent conformers; TS_3—transition state with chair conformation, TS_4—transition state with boat conformation; VIII—chemisorbed cyclohexene on Brønsted acid.

alkene, carbenium transition state and a chemisorbed alkane in the increasing order of their proximity to the active site. Hence, for the reaction involving physisorbed species as reactants and carbenium transition states, we expect higher activation barriers for embedded cluster calculations compared with bare cluster calculations. On the contrary, reactions involving chemisorbed species as reactants would result in lower activation energies for EC calculations. With increasing size of the QM portion, the residual repulsion is expected to become less significant and the difference between the activation energy for BC and EC calculations should decrease. In the case of the full QM calculation, like periodic DFT, the van der Waals interaction is expected [74,75] to provide a constant shift in the potential energy surface.

From a comparison of the activation barriers for two-step sequential chemisorption (EC 25.35 kcal/mol) and cyclization (EC 17.69 kcal/mol) with the alternative concerted pathway (EC 26.60 kcal/mol), we conclude that simultaneous protonation-cyclization will be a competing reaction pathway for cyclization starting from the physisorbed 1,5-hexadiene. However, for propane aromatization, a primary alkoxide intermediate can be generated via other reaction paths like hydride transfer or beta scission. After the formation of the chemisorbed primary alkoxide, the actual ring closure step has a lower activation barrier.

3.2. 1,5 cyclization of C6 diene

According to the classical view of cyclization, 1,5 ring closure is expected to be less activated than 1,6 ring closure since it avoids the formation of a primary carbenium intermediate for the cyclization of hexadiene. Concerted adsorption of an alkene has been extensively studied [41,63]. For completeness, we investigated the chemisorption of the 1,5-hexadiene starting from the physisorbed hexadiene on the Brønsted site at the Si12–O24–Al12 position. For the bare cluster calculation we find an activation barrier of 16.99 kcal/mol. Our investigations of 1,5 ring closure started with a secondary alkoxy species (IX in Fig. 11) formed by chemisorption of 1,5-hexadiene. For comparison with the 1,6 cyclization reaction pathway, we reported the reaction path (Fig. 12a) on the same energy scale (as in Figs. 3, 6, and 9). For easier interpretation we locate the physisorbed precursor for the secondary chemisorbed alkoxide along the reaction path shown in Fig. 12a. Of the several possible conformers we present, the case of 1,5 cyclization for the secondary alkoxide (IX) representing the path with the least possible steric hindrance, as shown in Fig. 11a. The product of cyclization (X) is shown in Fig. 11b. The transition state of the 1,5 cyclization is secondary carbenium ionic in nature. For the EC model, we calculated an activation barrier of 22.12 kcal/mol (BC: 23.32 kcal/mol). This activation energy is higher than that for 1,6 ring closure for hexadiene (EC: 17.7 kcal/mol). This result is surprising since according to carbenium chemistry rules the reaction path involving the secondary carbocationic transition state should be less activated. In Scheme 3, the 1,5 ring closure mechanism is located by an arrow between block B and block C (chemisorbed C5 cyclic alkenes).

As explained in the previous sections, after 1,5 ring closure the charge center shifts from C1 to the C4 position (Fig. 11). The downhill path after cyclization should involve several less energetically significant conformational adjustments and should lead to chemisorbed methylcyclopentene. The chemisorption site will involve a different oxygen atom than the original bridge oxygen for the acyclic precursor (T12–O20–T11). However, to estimate the correct energy of reaction we selected T12–O24–T12 as the chemisorption site for the cyclic product (X). Table 4 summarizes the key geometry and the charge parameters for the precursor (IX), transition state (TS_6), and product of 1,5-cyclization (X).

We observe four important peculiarities of the transition state for 1,5 ring closure. (1) The transient hydrocarbon species is more cationic than the corresponding transition states for 1,6 ring closure for hexadiene. It carries a total charge of 0.848 au, whereas the 1,6 cyclization analogue exhibits a charge of 0.770 au for hexadiene (TS_4). (2) The transition-state geometry exhibits a higher C1–O20 bond distance than the corresponding transition states for 1,6 cyclization. For TS_6 we observed a distance of 3.046 Å, and for the structure TS_4 we observed 2.362 Å. We conclude that the charge separation in the case of 1,5 cyclization results

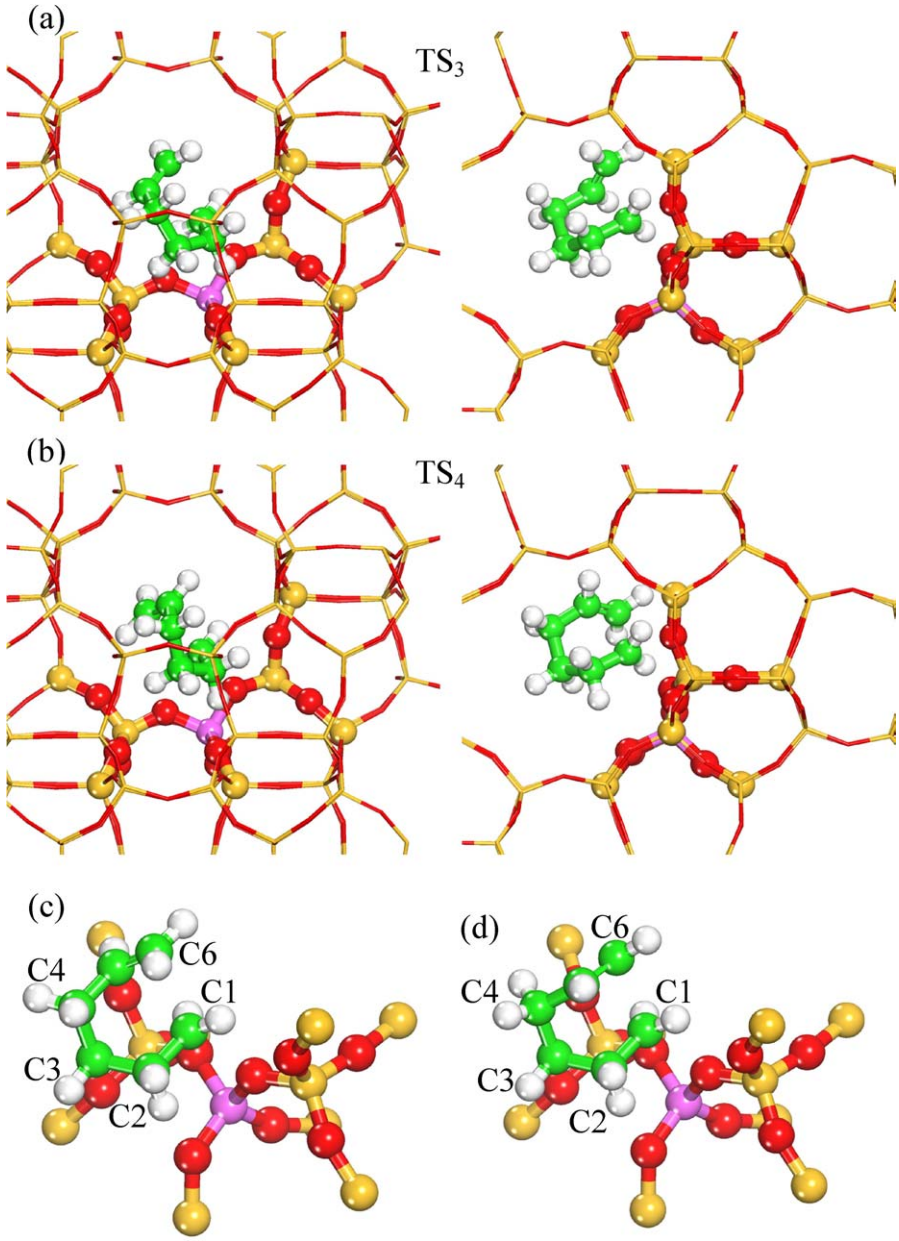

Fig. 7. Two conformers of the transition state for 1,6 ring closure of chemisorbed 1,5-hexadiene as primary alkoxide, (a) chair conformation; (b) boat conformation; (c) and (d) corresponding transition states for bare cluster calculations.

in the observed higher activation energy. (3) In the transition state structure, we observe significant positive charge at the C4 and C5 centers away from the terminal C=C double bond. (4) The C1–C5 atomic distance (the bond formed during cyclization) in the transition state is shorter than that in TS_4 (2.221 vs 2.393 Å). All of these observations indicate that the transition state for 1,5 ring closure (TS_6) is farther along the ring closure reaction path than the 1,6 ring closure transition state (TS_4) on its reaction paths. We believe that the fact that the transition state for 1,5 ring closure is farther along the reaction path and the fact that it is more activated than the 1,6 ring closure TS are related. 1,5 ring closure of the secondary surface alkoxide should cause significantly higher strain in the 5C chain (ring in formation) than that in the 6C chain for 1,6 cyclization of the primary surface alkoxide. To reduce this strain by conformational adjustment, the hydrocarbon species must move farther from the active site. This causes extra charge separation, which, in response, makes the overall reaction path more activated than expected. This correlation between the activation barrier and the location of the transition state along the reaction path has previously been observed for the chemisorption of various alkenes by Boronat et al. [41]. In their investigation of protonation with hybrid molecular simulation methods, they point out linear correlations between E_{act} and qH, qC$^+$, rOH, and rC=C.

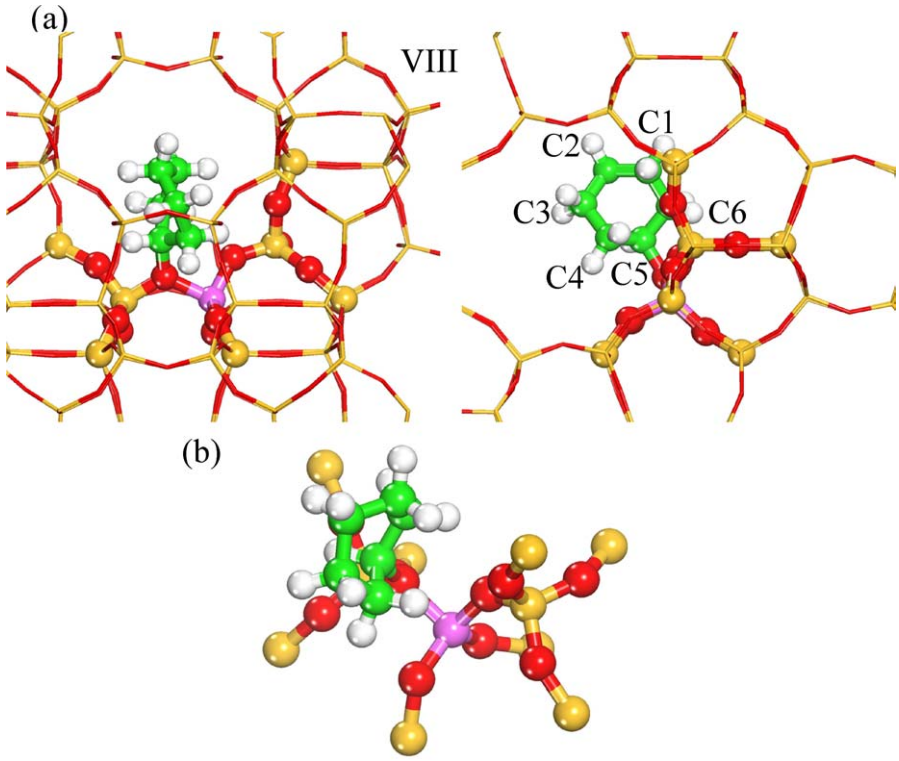

Fig. 8. Chemisorbed cyclohexene (VIII) on T12–O24–T12 bridge, (a) embedded cluster geometry; (b) bare cluster geometry.

Table 2
Important geometry and charge parameters for chemisorbed 1,5-hexadiene (VI, VII), TS for cyclization (TS_3, TS_4) and chemisorbed cyclohexene (VIII)[a]

	VI	VII	TS_3	TS_4	VIII
O20/24–C1/5[b] (Å)	1.515 (1.511)	1.521 (1.512)	2.290 (2.249)	2.362 (2.245)	1.550 (1.542)
T12–O20 (Å)	1.842 (1.857)	1.845 (1.857)	1.714 (1.749)	1.735 (1.750)	1.684 (1.704)
T12–O24 (Å)	1.688 (1.692)	1.688 (1.692)	1.709 (1.715)	1.712 (1.715)	1.845 (1.851)
C1–C2 (Å)	1.528 (1.521)	1.525 (1.519)	1.476 (1.480)	1.484 (1.480)	1.535 (1.535)
C1–C6 (Å)	3.573 (3.765)	3.285 (3.344)	2.513 (2.515)	2.393 (2.461)	1.549 (1.548)
T12–O20–C1/5[b] (deg)	112.2 (115.3)	110.3 (115.2)	104.7 (106.9)	104.7 (106.9)	120.1 (119.7)
O20–C1–C2 (deg)	109.4 (110.4)	111.7 (110.0)	103.1 (104.0)	100.9 (104.1)	–
Charge on C1[c]	0.375 (0.354)	0.368 (0.353)	0.370 (0.375)	0.352 (0.360)	0.014 (0.016)
Charge on C5[c]	0.068 (0.066)	0.038 (0.043)	0.108 (0.103)	0.068 (0.057)	0.301 (0.300)
Charge on C6[c]	−0.051 (−0.054)	−0.033 (−0.043)	0.038 (0.035)	0.099 (0.084)	0.067 (0.064)
Total HC charge	0.453 (0.450)	0.448 (0.445)	0.741 (0.732)	0.770 (0.745)	0.468 (0.465)

[a] Bracketed quantities represent bare cluster calculations and the ones without brackets represent embedded cluster calculations.
[b] Geometry parameters after '/' represent structure VIII.
[c] Mulliken charges of bonded hydrogens summed into carbon charge.

3.3. *Ring expansion of methylcyclopentene*

Ring enlargement reactions are important for the selective control of ring size. These reactions are used in the synthesis of macrocyclic compounds, with commercial importance in the fragrance and pharmaceutical industry. On the basis of structural transformation, ring expansion mechanisms can be classified into three categories, as shown in Scheme 4 [76]. The author points out that after consideration of the intermediates and transition states along the reaction path, Scheme 4a involving a bicyclic intermediate, can be generalized as a regular ring expansion mechanism. Our results agree with this hypothesis [76]. In our previous work [37] we showed that the gas-phase methylcyclopenta carbenium ion can undergo ring expansion via two pathways: (1) starting from a tertiary carbenium ion, ring expansion involving a primary carbenium ion, with a higher activation barrier, and (2) starting from a secondary carbenium ion (IUPAC: 2-methylcyclopent-1-ylium), ring expansion via bicyclic transient intermediate. The effective secondary nature of this transition state results in lower ring expansion activation energy compared to the one starting from a tertiary carbenium species. Along similar lines we present the ring expansion mechanism in the zeolite with two possible reaction paths.

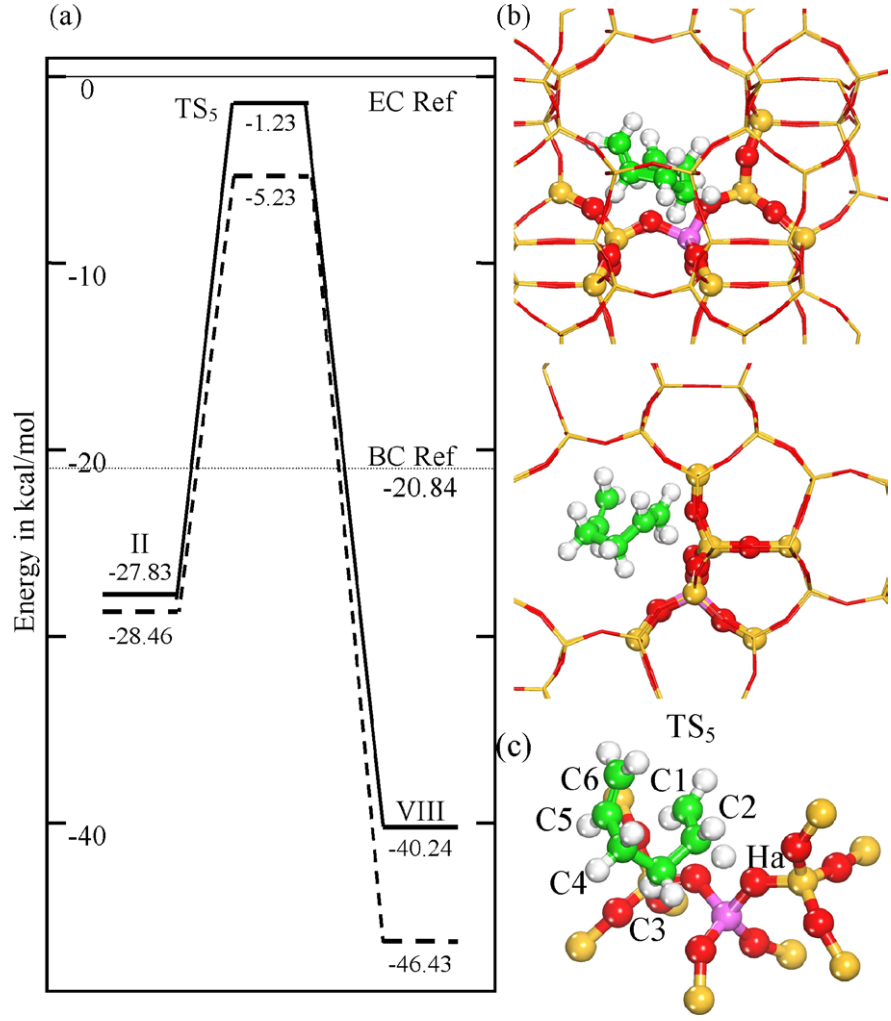

Fig. 9. (a) Reaction path for concerted 1,6 ring closure and protonation of the bent physisorbed diene II—bent physisorbed diene; TS_5—transition state for protonation and ring closure; VIII—cyclohexene chemisorbed at T12–O24–T12; (b) TS geometry for EC calculation, both views; (c) TS geometry for BC calculation.

Table 3
Geometry and charge parameters for the physisorbed bent hexadiene (II) and transition state (TS_5) for simultaneous ring closure and protonation[a]

	II	TS_5
O20–HA (Å)	0.991 (0.996)	1.505 (1.484)
C1–HA (Å)	2.189 (2.096)	1.933 (1.912)
C2–HA (Å)	2.369 (2.275)	1.249 (1.249)
T12–O20 (Å)	1.832 (1.833)	1.752 (1.753)
T12–O24 (Å)	1.688 (1.693)	1.709 (1.715)
C1–C2 (Å)	1.340 (1.342)	1.401 (1.398)
C1–C6 (Å)	4.492 (4.527)	2.640 (2.626)
T12–O20–HA (deg)	111.2 (111.3)	108.8 (107.1)
Charge on C1[b]	−0.041 (−0.047)	0.255 (0.275)
Charge on C2[b]	0.076 (0.075)	0.221 (0.217)
Charge on C6[b]	−0.057 (−0.060)	0.007 (0.007)
Charge on Ha	0.385 (0.383)	0.345 (0.338)
Total HC charge	0.079 (0.080)[c]	0.745 (0.756)[d]

[a] Bracketed quantities represent bare cluster calculations and the ones without brackets represent embedded cluster calculations.
[b] Mulliken charges of bonded hydrogens summed into carbon charge.
[c] Without counting Brønsted proton in the hydrocarbon.
[d] After counting proton in the hydrocarbon.

According to acid-catalyzed hydrocarbon chemistry, the ring expansion mechanism can be simply classified as an isomerization reaction, and a general branching isomerization can occur by two paths: (1) an alkyl shift mechanism involving a shift in the alkyl species from the β position to the α position (naturally the alkoxide center will shift from the α carbon to the β carbon; however, manipulation of the electron-deficient alkyl species in the alkoxide structure is expected to be energetically unfavorable) and (2) another reaction pathway involving a cyclopropyl intermediate. There has been experimental evidence for the cyclopropyl intermediate by ^{13}C labeling [77]. Recently Demuth et al. [78] reported periodic DFT investigation of the 2-pentene isomerization. Their results are in agreement with this classical understanding and suggest the possibility of an edge protonated dimethylcyclopropane (DMCP) intermediate. A ring expansion can be perceived as a reverse reaction to branching isomerization. However, the extra constraint of the cyclopentyl ring makes this problem interesting for current investigation.

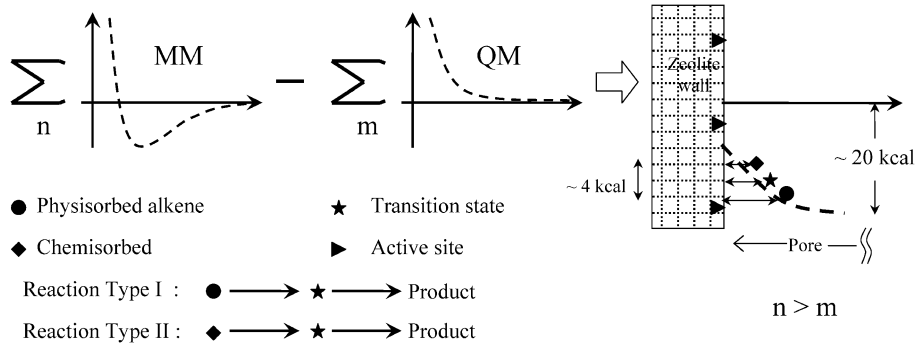

Fig. 10. Schematic diagram explaining the effect of the van der Waal's forces on potential energy surface of hydrocarbon transformation using finite cluster model of the site.

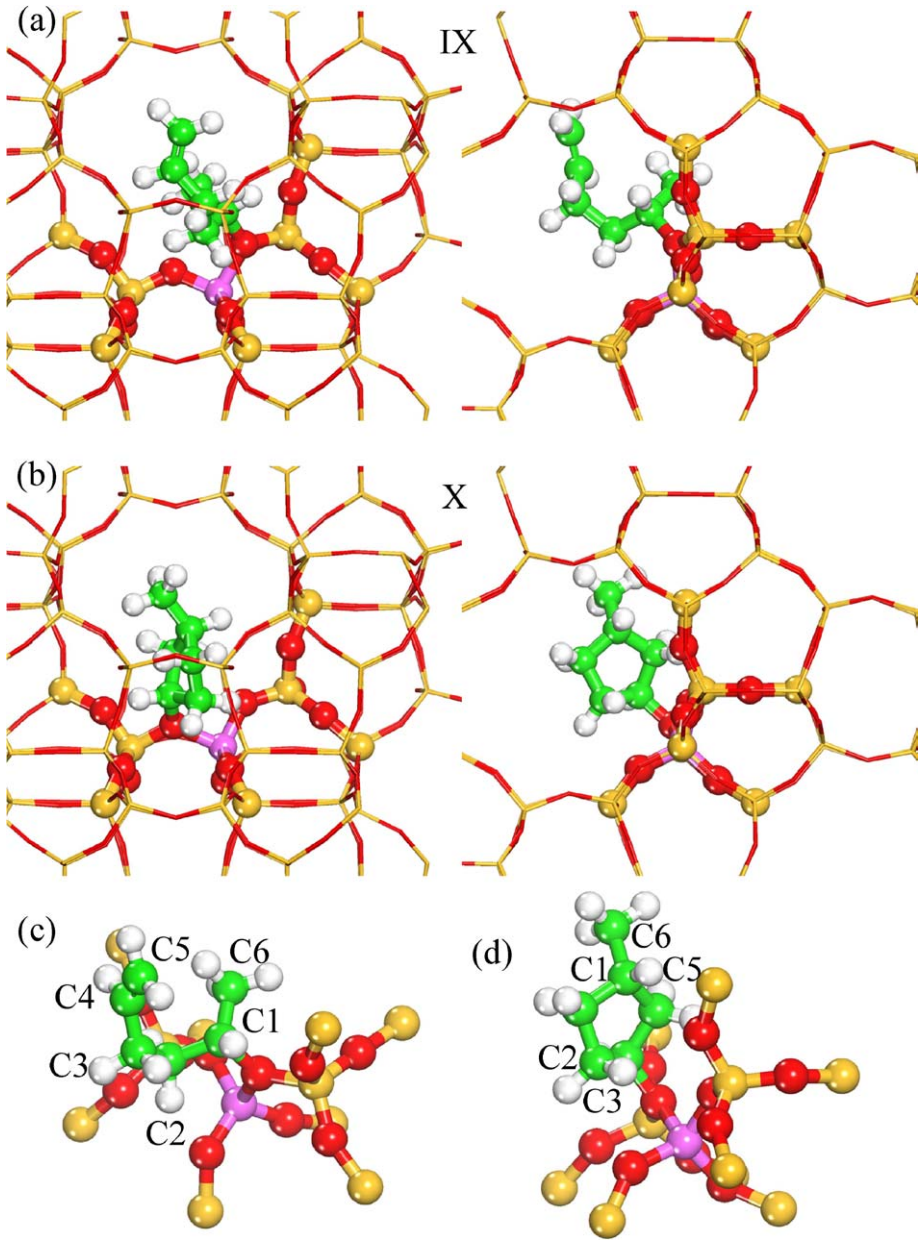

Fig. 11. (a) Chemisorbed secondary alkoxide (IX) of 1,5-hexadiene on T12–O20–T11 bridge; (b) product after cyclization, chemisorbed methyl cyclopentene (X) on T12–O24–T12 bridge; (c) and (d) bare cluster analogues for (a) and (b).

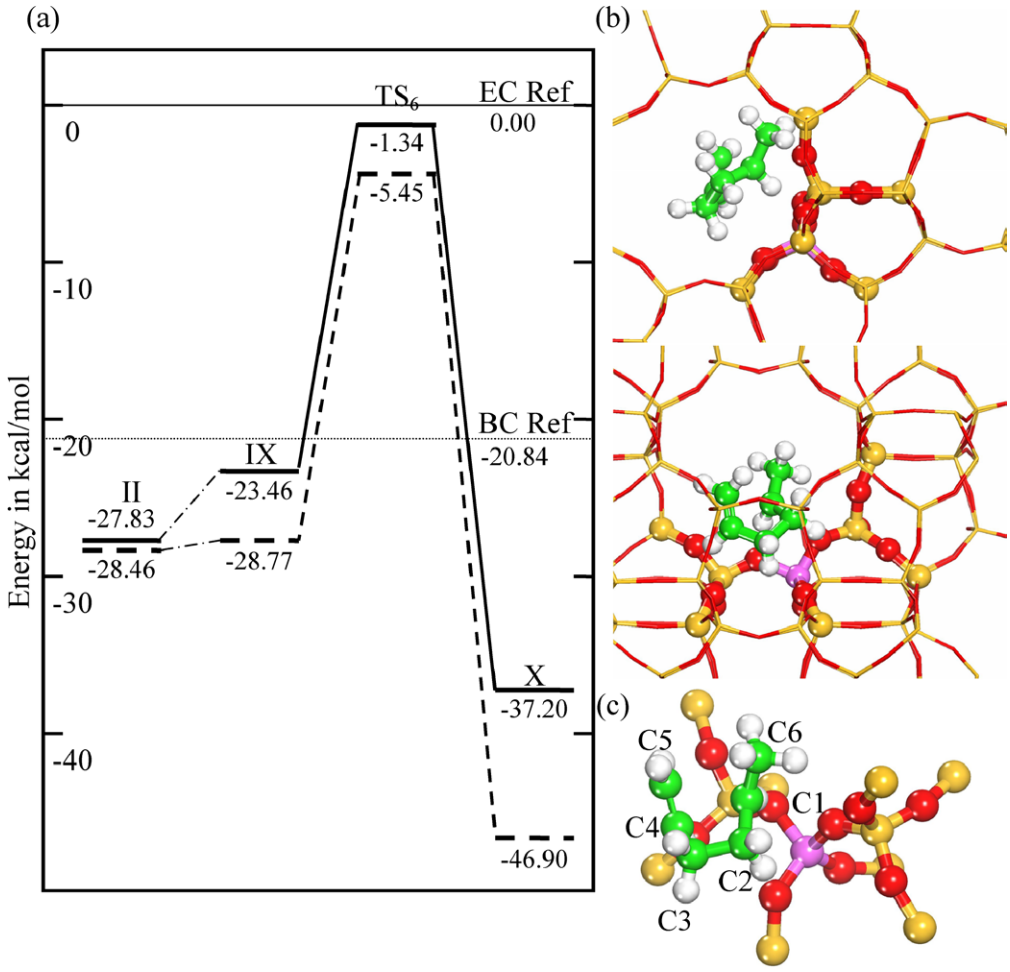

Fig. 12. (a) Reaction path for 1,5 ring closure for chemisorbed secondary alkoxide (1,5-hexadiene), II—physisorbed hexadiene; IX—chemisorbed secondary alkoxide; TS_5—transition state for 1,5 ring closure; X—methylcyclopentene chemisorbed on T12–O24–T12; (b) transition state geometry; (c) bare cluster analogue of (b).

Table 4
Geometry and charge parameters for chemisorbed 1,5-hexadiene-secondary alkoxide (IX), TS for 1,5 cyclization (TS_6) and chemisorbed methylcyclopentene (X) secondary alkoxide[a]

	IX	TS_6	X
O20/24–C1/5[b] (Å)	1.576 (1.547)	3.046 (2.950)	1.529 (1.524)
T12–O20 (Å)	1.852 (1.860)	1.715 (1.720)	1.685 (1.705)
T12–O24 (Å)	1.685 (1.692)	1.721 (1.726)	1.838 (1.849)
C1–C5 (Å)	4.077 (3.857)	2.221 (2.462)	1.562 (1.561)
T12–O20-C1/5 (deg)	118.0 (119.7)	95.9 (92.5)	118.2 (119.2)
O20–C1–C2 (deg)	111.2 (111.0)	91.1 (91.7)	–
T12–O20–C1–C6 (deg)	−93.2 (−93.7)	−151.9 (−152.3)	–
Charge on C1[c]	0.322 (0.319)	0.236 (0.288)	0.043 (0.047)
Charge on C4[c]	0.076 (−0.052)	0.156 (0.121)	0.282 (0.298)
Charge on C5[c]	−0.054 (−0.011)	0.079 (0.036)	0.066 (0.057)
Total HC charge	0.463 (0.453)	0.848 (0.836)	0.446 (0.458)

[a] Bracketed quantities represent bare cluster calculations and the ones without brackets represent embedded cluster calculations.
[b] Geometry parameters after '/' represent structure X.
[c] Mulliken charges of bonded hydrogens summed into carbon charge.

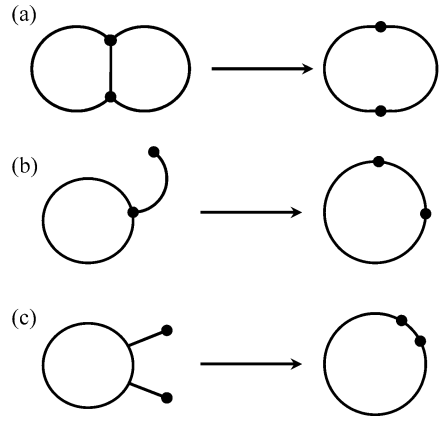

Scheme 4. Principal structural transformations for ring expansion [64].

For ring expansion via the alkyl shift mechanism, we started with a primary alkoxide (XI) as shown in Fig. 13a. Formation of the primary alkoxide from the secondary alkoxide (X) involves several hydride shifts. Considering this pathway as a Brønsted acid site-catalyzed mechanism, we expect it to involve several sequential alkene

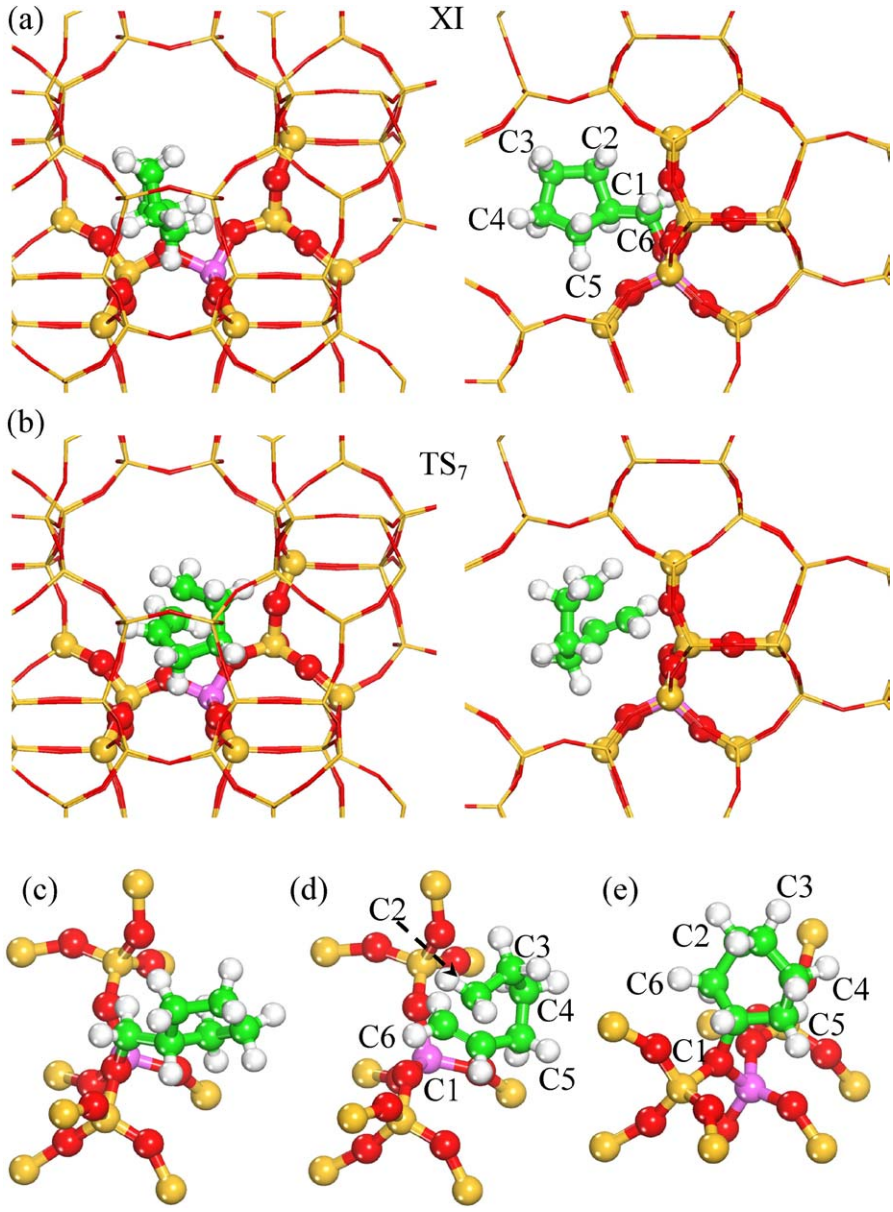

Fig. 13. (a) Chemisorbed primary alkoxide (XI) of methylenecyclopentane on T12–O24–T12 bridge; (b) transition state (TS_7) for ring expansion by alkyl shift isomerization mechanism; (c) and (d) bare cluster analogues for (a) and (b); (e) chemisorbed cyclohexene (VIII as in Fig. 8b with different carbon numbering scheme).

desorption and re-adsorption steps, such that the alkoxide center will shift as [C4,Secondary] → [C5,Secondary] → [C1,Tertiary] → [C6,Primary]. As described in our previous publication [37], we find that the primary alkoxide (XI) is more stable than the secondary alkoxide (X). This stability order reversal is interpreted as the effect of higher steric repulsion toward the secondary carbon compared with primary carbon. However, it is well known that formation of the primary alkoxide is much more activated compared with the secondary or tertiary alkoxide.

Based on our computational results, the alkyl shift starting from XI involved breaking of the C2–C1 bond and simultaneous bond formation between C2–C6. Thus the transition-state structure (TS_7) is triangular, comprising C1, C2, and C6. Bond distances for C2–C1 and C2–C6 were 1.875 and 1.844 Å, respectively. These distances are slightly longer that the ones reported by Demuth et al.; however, strain due to the 5-member ring could be a reason for this elongation. Relevant geometry and charge parameters are listed in Table 5. As shown in Fig. 14, our calculated activation barrier for the EC model is 29.31 kcal/mol (BC: 28.28 kcal/mol). This activation energy agrees with the value of ∼ 29 kcal/mol reported by Demuth et al. [78] for the reverse of branching isomerization. However, this agreement could be coincidental, since the energy of reaction for ring expansion is drastically different from that for isomerization reported by Demuth et al. Both calculations signify the effect of the pore geometry on the stability of

Table 5
Geometry and charge parameters for chemisorbed methylenecyclopentane-primary alkoxide (XI), TS for ring expansion by alkyl transfer mechanism (TS_7) and chemisorbed cyclohexene (VIII)[a]

	XI	TS_7	VIII[b]
O24–C6 (Å)	1.522 (1.515)	2.655 (2.594)	2.508 (2.500)
O24–C1 (Å)	2.552 (2.545)	3.245 (3.162)	1.550 (1.544)
T12–O24 (Å)	1.846 (1.857)	1.719 (1.724)	1.845 (1.851)
T12–O20 (Å)	1.682 (1.703)	1.718 (1.721)	1.684 (1.704)
C2–C1 (Å)	1.556 (1.555)	1.875 (1.874)	2.534 (2.530)
C2–C6 (Å)	2.517 (2.506)	1.844 (1.845)	1.549 (1.548)
C1–C6 (Å)	1.517 (1.517)	1.390 (1.389)	1.531 (1.530)
C1–C2–C6 (deg)	34.5 (34.8)	43.9 (43.9)	34.4 (35.0)
C2–C1–C6 (deg)	110.0 (109.3)	66.9 (66.9)	34.8 (34.5)
Charge on C6[c]	0.360 (0.339)	0.329 (0.321)	0.067 (0.064)
Charge on C1[c]	0.008 (0.026)	0.133 (0.146)	0.301 (0.300)
Charge on C2[c]	0.001 (0.001)	0.071 (0.066)	0.014 (0.016)
Total HC charge	0.440 (0.437)	0.856 (0.837)	0.468 (0.465)

[a] Bracketed quantities represent bare cluster calculations and the ones without brackets represent embedded cluster calculations.
[b] As labeled in the Fig. 13e.
[c] Mulliken charges of bonded hydrogens summed into carbon charge.

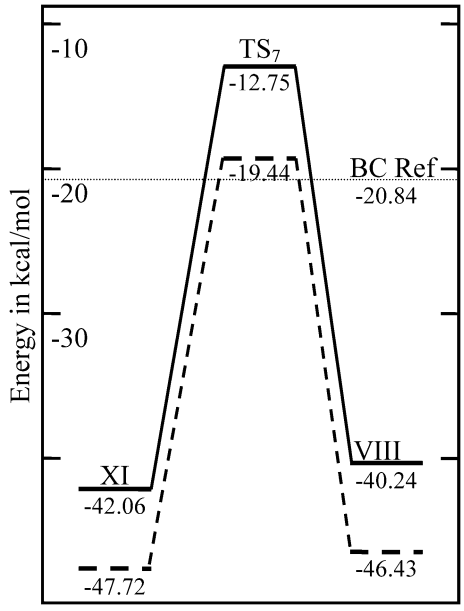

Fig. 14. Reaction path for ring expansion by alkyl shift isomerization mechanism, XI—primary methylenecyclopentane alkoxide; TS_7—transition state for ring expansion; VIII—cyclohexene chemisorbed on T12–O24–T12.

the reactant or product. Significant positive charge on the transient hydrocarbon species indicates the carbenium nature of the transition state. Considering the activation barrier for ring expansion by alkyl mechanism, we conclude that the migration of the alkoxide center to the primary carbon should be rate determining. However, near equilibrium the higher concentration of the primary alkoxides should make this pathway competitive. A more extensive study of pathways involving more than just one cyclic C5 conformer is needed.

Another possible reaction path for ring expansion involves the dialkylcyclopropane intermediate. This reaction path starts with a secondary alkoxide of methylcyclopentene (XII) as shown in Fig. 15a. The distance between C5 and C6 decreases with decreasing angle C5–C1–C6. The methyl group at the C6 position loses a proton to O24, forming a Brønsted acid site. Simultaneously, there is bond formation between C5 and C6, resulting in bicyclo[3.1.0]hexane. It is well known [79] that the strain in the cyclopropyl ring induces the π-character to C–C covalent bonds. Hence cyclopropyl intermediates physisorb (XIV) on Brønsted acid sites. Just before the formation of the bicyclic intermediate we found an inflection point (XIII) on the potential energy surface. This intermediate transforms into the bicyclo intermediate by an unactivated process. Such inflection points on the potential energy surface involving higher hydrocarbons have been reported previously [74,75].

The reaction path and transition state (TS_8) for this portion of the ring expansion pathway are shown in Figs. 16 and 17, respectively. The activation barrier for the formation of bicyclo[3.1.0]hexane is 20.12 kcal/mol for the EC model and 20.34 kcal/mol for the BC calculation. However, the main difference between the two calculations is the energy change for the reaction. The EC calculation showed the reaction to be exothermic ($\Delta E < 0$), whereas for the BC it is endothermic. This observation is explained by the expected higher stabilization of the physisorbed product due to van der Waals interaction in the EC model. In Table 6 we report the geometry and charge parameters for the intermediates involved in the mechanism. A charge of 0.82 au marks the transition state TS_8 as carbocationic; at the same time this charge is well distributed between C5 and C6. Since the bicyclic intermediates are compact and rigid, the effect of the embedded cluster environment on the hydrocarbon geometry is minimal.

We propose that this bicyclo[3.1.0]hexane intermediate should desorb and re-adsorb as structure XV shown in Fig. 18. For the BC calculation the physisorbed geometry of XV indicates π-interaction between the C1–C5 bond and the Brønsted acid site. However, for the EC calculation the zeolite channel constraint moves the hydrocarbon species farther from the Brønsted acid site. The C1–Ha and C5–Ha distances are 3.684 and 3.844, respectively (BC: 2.405 and 2.559 Å). The C1–C5 bridge bond undergoes protolytic scission to form the 6C cyclic product (XVII). In the bare cluster we found two transition-state geometries for breaking the C1–C5 bridge bond shown as TS_9 and TS_{10} in Fig. 17. In TS_9 the C1–C5 bridge bond is directed along the sinusoidal channel, whereas in TS_{10} it is parallel to the straight channel. However, because of the extended pore structure, the EC calculations show transition-state shape selectivity toward TS_9. We found that transition state TS_{10} geometry was destabilized in our EC calculation, and hence in Fig. 16 we present the reaction path without TS_{10}. The EC calculated activation barrier for the second step of the ring expansion mechanism was 21.31 kcal/mol (BC: 16.57 kcal/mol). Since this

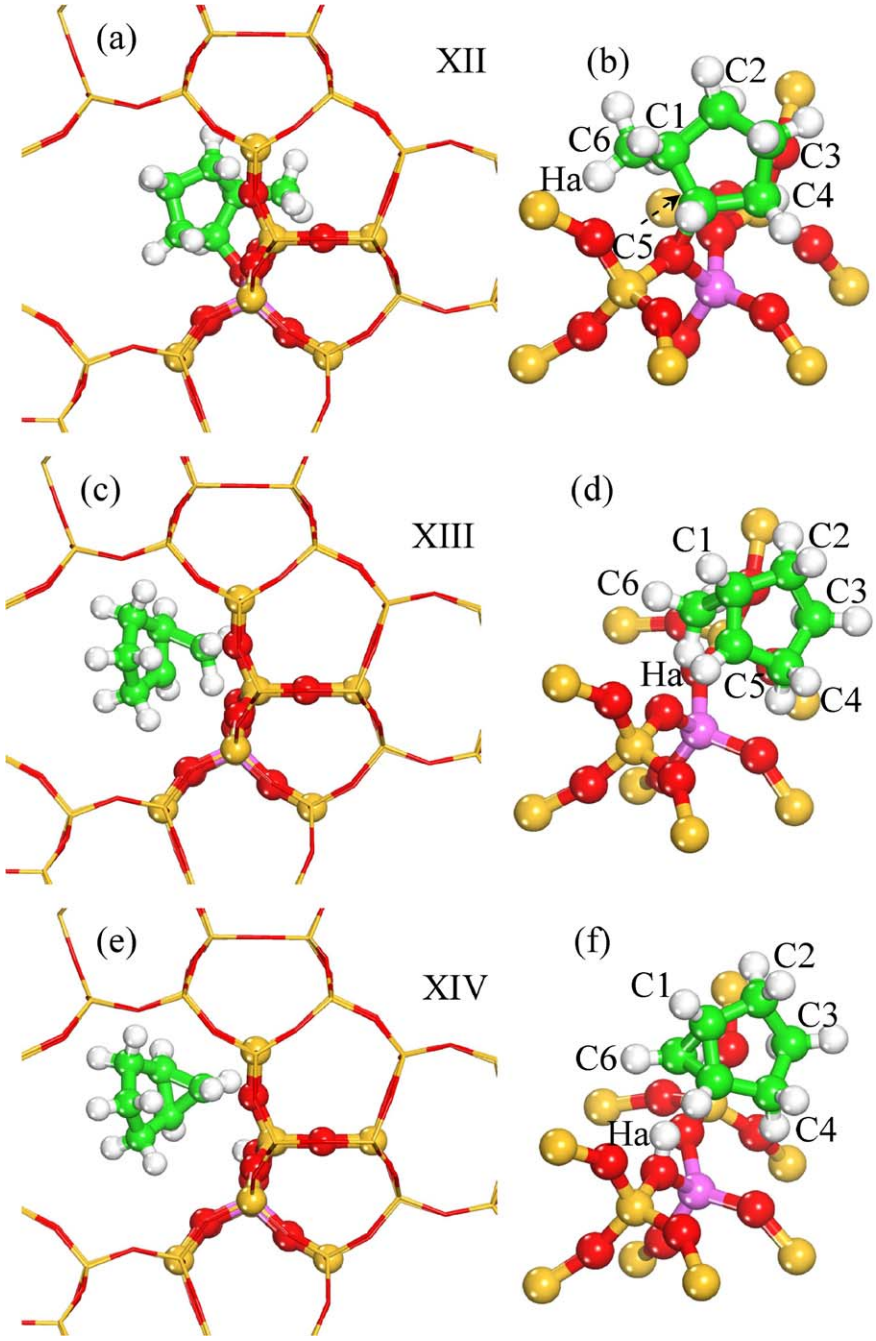

Fig. 15. Intermediates along the reaction path for formation of the bicycle[3.1.0]hexane (a) secondary alkoxide (XII) of methylcyclopentene; (c) inflection point geometry (XIII) before formation of bicyclohexane; (d) bicyclohexane physisorbed (XIV) on Brønsted acid site; (b), (d) and (f) bare cluster analogues of (a), (c) and (e), respectively.

reaction step involves a physisorbed reactant, the activation barrier for the EC model was higher than that for the BC model. For this reaction path also, we observe a stable carbenium species (XVI) along the downhill reaction path. A comparison of the two mechanisms for ring expansion clearly suggests that the ring expansion via bicyclohexane is kinetically more favorable. This mechanism involves only secondary alkoxides, compared with primary alkoxides for ring expansion by alkyl transfer.

4. Conclusions and summary

We have studied the cyclization of 1,5-hexadiene to form C6 cyclic alkoxides in HZSM-5 with the use of hybrid embedded-cluster techniques. Using an embedded-cluster model of the active site at the T12 position, we have calculated physisorption energies of 28.43 and 28.67 kcal/mol, respectively, for bent and linear conformations of the hexadiene. These energies are in better agreement with the

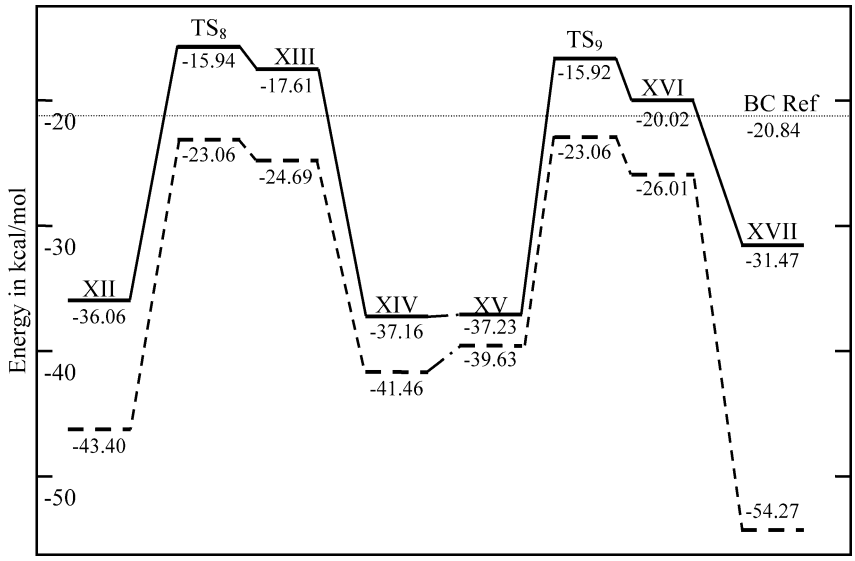

Fig. 16. Reaction path for ring expansion via bicyclo[3.1.0]hexane, XII—secondary methylcyclopentene alkoxide; TS_8—transition state for the formation of the bicyclo intermediate; XIII—inflection point on reaction path; XIV—bicyclohexane physisorbed on Brønsted acid site at T12–O24–T12; XV—readsorbed bicyclohexane with different orientation; TS_9—transition state for protolytic scission of the C1–C5 bridge bond; XVI and XVII—species along the downhill path to cyclohexene chemisorbed on T12–O11–T11.

Table 6
Geometry and charge parameters for chemisorbed methylcyclohexene (XII), TS for formation of bicyclohexane (TS_8), several bicyclo intermediates (XIII, XIV, XV), TS for breaking C1–C5 bridge bond (TS_9) and 6C cyclic products (XVI, XVII)[a]

	XII	TS_8	XIII	XIV	XV	TS_9	XVI	XVII
O24/11[b]–C5 (Å)	1.536 (1.530)	3.086 (3.050)	3.050 (3.107)	3.475 (3.231)	3.928 (3.930)	3.568 (3.773)	3.093 (3.083)	1.636 (1.537)
O24–Ha (Å)	2.843 (1.093)	2.210 (2.139)	1.626 (1.736)	0.977 (0.985)	0.969 (0.978)	1.421 (1.430)	2.048 (1.964)	–
T12–O24 (Å)	1.846 (1.857)	1.721 (1.728)	1.743 (1.741)	1.830 (1.835)	1.830 (1.838)	1.765 (1.770)	1.716 (1.725)	1.676 (1.685)
T12–O20 (Å)	1.685 (1.704)	1.705 (1.715)	1.707 (1.717)	1.690 (1.703)	1.693 (1.704)	1.703 (1.717)	1.713 (1.716)	1.677 (1.692)
C1–C6 (Å)	1.530 (1.530)	1.623 (1.624)	1.590 (1.609)	1.515 (1.513)	1.511 (1.510)	1.560 (1.551)	1.674 (1.660)	1.544 (1.542)
C1–C5 (Å)	1.566 (1.563)	1.440 (1.437)	1.438 (1.429)	1.510 (1.507)	1.510 (1.534)	1.666 (1.672)	1.931 (1.909)	2.516 (2.514)
C6–C5 (Å)	2.660 (2.638)	2.225 (2.210)	1.735 (1.784)	1.526 (1.536)	1.520 (1.505)	1.452 (1.455)	1.408 (1.411)	1.522 (1.524)
C6/1[b]–Ha (Å)	1.093 (1.093)	1.099 (1.099)	1.198 (1.160)	2.452 (2.153)	3.684 (2.405)	1.815 (1.772)	2.151 (1.114)	1.095 (1.095)
C5–Ha (Å)	2.964 (2.950)	2.221 (2.215)	1.758 (1.794)	2.737 (2.390)	3.844 (2.559)	1.319 (1.327)	1.105 (2.005)	–
C6/1[b]–C1/6[b]–C5 (deg)	118.4 (117.1)	93.0 (92.3)	69.1 (71.6)	60.6 (61.1)	60.4 (61.1)	67.1 (67.5)	77.1 (76.4)	111.2 (110.2)
Charge on C1[c]	0.032 (0.033)	0.004 (0.008)	0.047 (0.050)	−0.018 (−0.021)	−0.002 (−0.024)	0.289 (0.288)	0.171 (0.172)	0.008 (0.008)
Charge on C5[c]	0.303 (0.305)	0.310 (0.315)	0.125 (0.158)	−0.013 (−0.014)	0.019 (−0.004)	0.112 (0.108)	0.243 (0.236)	0.274 (0284)
Charge on C6[c]	0.019 (0.022)	0.209 (0.204)	0.358 (0.328)	−0.024 (−0.022)	−0.019 (0.013)	0.113 (0.115)	0.169 (0.162)	0.057 (0.056)
Charge on proton (Ha)	–	–	–	0.398 (0.408)	0.386 (0.389)	–	–	–
Total HC charge	0.445 (0.447)	0.825 (0.822)	0.785 (0.807)	0.018 (0.030)[d]	0.000 (0.022)[d]	0.699 (0.709)	0.834 (0.823)	0.472 (0.461)

[a] Bracketed quantities represent bare cluster calculations and the ones without brackets represent embedded cluster calculations.
[b] Geometry parameters after '/' represent structure XV, TS_9, XVI and XVII.
[c] Mulliken charges of bonded hydrogens summed into carbon charge.
[d] Without counting Brønsted proton in hydrocarbon.

expected experimental value. Our calculations confirm a significant contribution of the van der Waals forces to the physisorption energies.

Our investigations cover 1,6 ring closure and 1,5 ring closure followed by ring expansion paths. We have found that the 1,6 cyclization can start from both chemisorbed and physisorbed 1,5-hexadiene. Since chemisorption can occur through a double-site mechanism (whereby two conjugate oxygens from the same T-site are involved, with the alkoxide forming on the alternate oxygen) or a single-site mechanism (where the alkoxide is formed on the original oxygen carrying a Brønsted proton), steric effects strongly determine how, if at all, the chemisorption will proceed. For example, starting from linear 1,5-hexadiene (III) physisorbed on the Brønsted acid site at T12–O20–T03, we find that the single-site mechanism leads to a primary alkoxide. This mechanism is feasible only if the rest of the hydrocarbon chain is constrained along the sinusoidal channel of the embedded cluster model. The activation barrier for this chemisorption mechanism was 36.02 kcal/mol. Furthermore, depending on which oxygen the Brønsted proton resides on, the physisorbed bent conformer may be inclined to undergo direct 1,6 ring closure, avoiding the chemisorbed acyclic alkoxide altogether, as was the case for bent conformer II. The activation barrier for this one-step mechanism was calculated to be 26.60 kcal/mol. The difference between conformers II and IV was in the identity of the oxygen (O20 versus O11) carrying the Brønsted proton, although in both cases aluminum

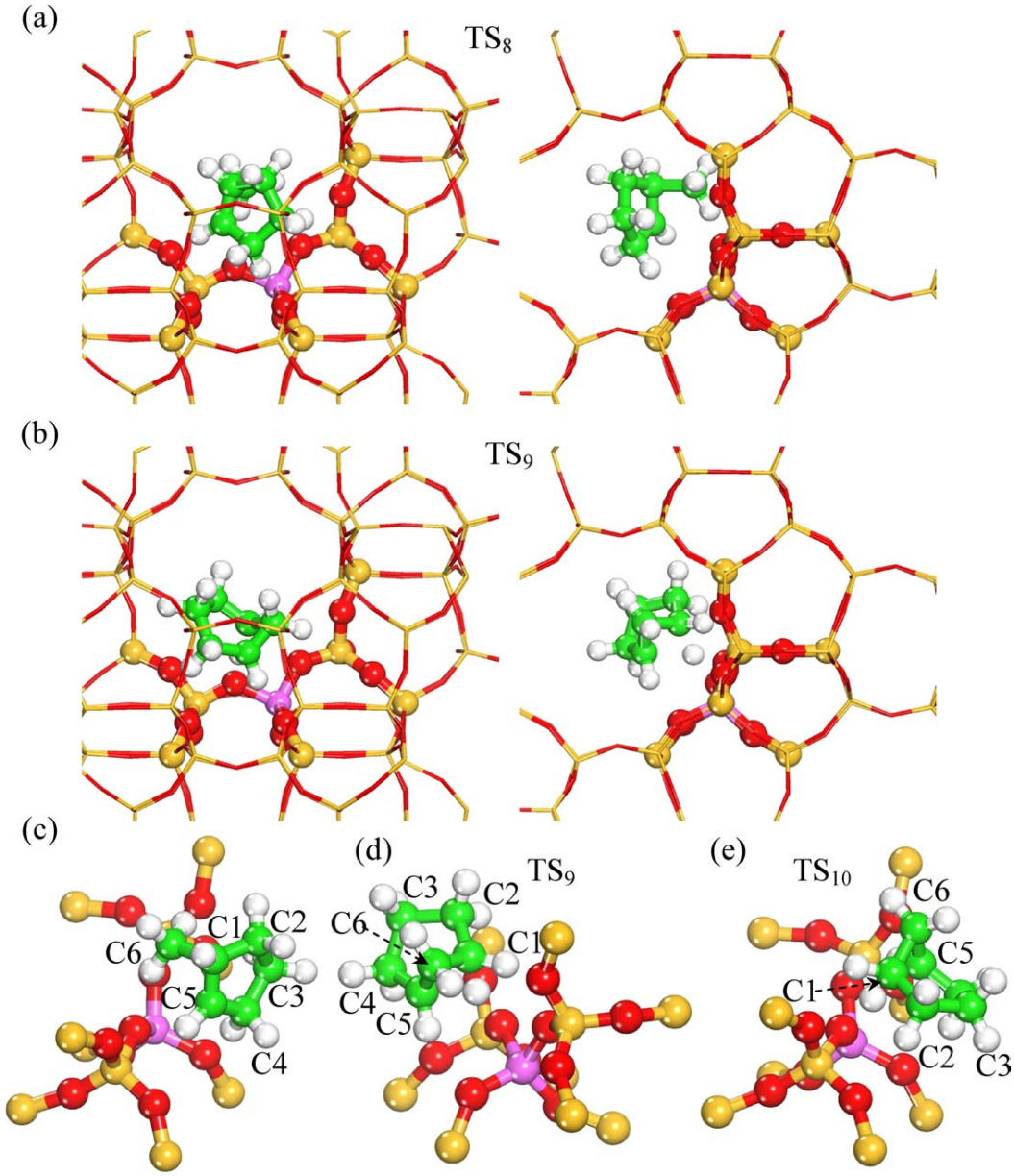

Fig. 17. (a) Transition state (TS_8) for the formation of the bicyclo intermediate; (b) transition state (TS_9) for the formation of cyclohexene chemisorbed from bicyclo intermediate; (c) and (d) are bare cluster structures corresponding to (a) and (b); (e) transition state (TS_{10}) for protolytic scission of C1–C5 bridge bond, observed only for BC.

was substituted at the T12 position. Conformer II, which, because of the absence of the second oxygen proximate to the primary carbon, would have been forced to chemisorb via a single-site mechanism, preferred to undergo direct cyclization. On the other hand, conformer IV preferred to first chemisorb via a double-site mechanism, and then undergo 1,6 ring closure. This double-site mechanism represents the least activated path ($E_{act} = 25.35$ kcal/mol) for chemisorption of the 1,5-hexadiene on the T12–O20–T03 oxygen to form a primary alkoxide.

Starting from the chemisorbed 1,5-hexadiene (primary or secondary), we observe that cyclization from chemisorbed alkoxides can occur by either direct 1,6 cyclization or through a combined mechanism of 1,5 cyclization followed by ring expansion. Direct 1,6 cyclization is preferred when reaction starts with a primary alkoxide; however, starting with a secondary alkoxide, only a 1,5 cyclization pathway is possible. We calculated an activation barrier of 17.7 kcal/mol for direct 1,6-cyclization from a primary alkoxide compared with 22.12 kcal/mol for 1,5-cyclization from a secondary alkoxide—despite the fact that the transition state in the 1,5 ring closure pathway is secondary carbocationic in nature, as opposed to the transition state for 1,6 cyclization, which is primary carbocationic. Strain in the 5C ring is responsible for this reversal, forcing greater charge separation of the hydrocarbon species from the con-

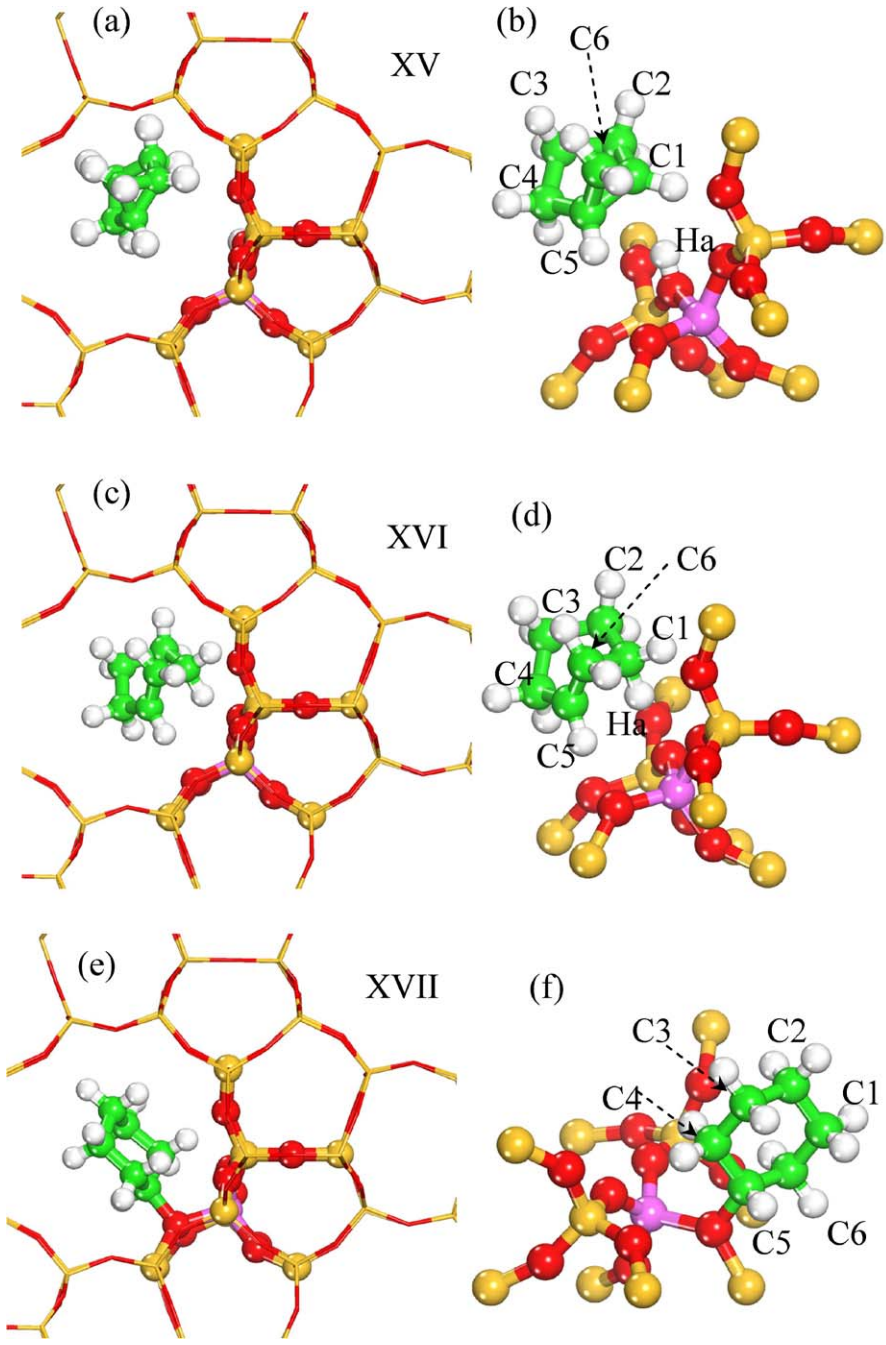

Fig. 18. Intermediates along the reaction path for formation of the cyclohexene chemisorbed starting from bicyclo[3.1.0]hexane: (a) bicyclohexane physisorbed on Brønsted acid site (XV); (c) inflection point geometry after C1–C5 bond cleavage; (e) secondary alkoxide of cyclohexene adsorbed at T12–O11–T11 (XVII); (b), (d) and (f) bare cluster analogues of (a), (c) and (e), respectively.

jugate base site, and hence greater cationic character relative to the primary transition state.

We found two pathways for C5 ring expansion. The more direct route involved hydride transfer via alkoxide desorption/readsorption, followed by ring expansion through a simultaneous alkyl shift/ring opening step. The second, energetically more favorable route involved the formation of a stable bicyclo[3.1.0]hexane intermediate, followed by ring expansion to a C6 alkoxide. The first route had an activation barrier of 29.31 kcal/mol, and the second route had an activation energy of 21.31 kcal/mol for its limiting step (lower than the 22.12 kcal/mol we observed for initial 1,5 ring closure). With our embedded cluster calculations we reconfirm the stability order reversal for alkoxide species, finding primary alkoxides to be more stable than secondary alkoxides. Thus near equilibrium, primary alkoxide species should dominate and 1,6 cyclization should be the observed cyclization path for *n*-hexadiene. However, it has been well

established that, because of the carbenium nature of transition states, the activation barriers for chemisorption to secondary alkoxides are smaller than those for primary alkoxides. Hence we suspect that for conditions far from equilibrium, secondary alkoxy species will dominate and the 1,5 ring closure and expansion mechanism will be feasible.

Finally, we show that embedded cluster calculations are essential for proper analysis of C6 olefin chemistry in ZSM-5 models. In particular we observe fairly important distinctions between embedded cluster and bare cluster results. Reactions starting from physisorbed states exhibit higher activation barriers in EC calculations compared with BC calculations, and the converse is true for reactions starting from chemisorbed species. In embedded cluster calculations, underlying van der Waals forces modify the potential energy surface for hydrocarbon transformations. The extent of the modifications depends on the nature of the hydrocarbon species. We also note that the extended pore structure modeled appropriately in our EC calculations resulted in either exclusion of some pathways originally observed in bare cluster calculations or inclusion of the new pathways due to added constraint. This was particularly true for the linear conformer, which had a tendency to align along the sinusoidal channel. For bare cluster calculations the absence of the constraints destabilized transition states. Furthermore, these constraints were also apparent with bent conformers. In this case, the constraint offered by the MFI pore structure reduces the C1–C6 distance of the chemisorbed hexadiene and pushes it farther along the reaction coordinate of 1,6 ring closure. This activation, in conjunction with stabilization of the transition state due to van der Waals interactions, reduces the activation barrier for 1,6 ring closure of the primary alkoxide in the case of the embedded cluster model. This type of site preference cannot be realized with bare cluster models.

Acknowledgments

We thank Prof. W. Nicholas Delgass and Aditya Bhan for enlightening discussions on zeolite-catalyzed hydrocarbon chemistry. This work was supported by the State of Indiana through a grant from the 21st Century Technology Fund, U.S. Department of Energy (DOE), Office of Basic Sciences (grant DE-FG02-03ER-15466) and through the National Science Foundation (grant CTS-0238989-CAREER). Computational resources were obtained through a grant (MCA04N010) from the National Computational Science Alliance (Machines: copper.ncsa.uiuc.edu and tungsten.ncsa.uiuc.edu) and through supercomputing resources at Purdue University.

References

[1] M.S. Scurrell, Appl. Catal. 32 (1987) 1.
[2] J.R. Mowry, R.F. Anderson, J.A. Johnson, Oil Gas J. 83 (1985) 128.
[3] N.Y. Chen, T.Y. Yan, Ind. Eng. Chem. Process Des. Dev. 25 (1986) 151.
[4] M. Guisnet, N.S. Gnep, F. Alario, Appl. Catal. A 89 (1992) 1.
[5] Y. Ono, Catal. Rev.-Sci. Eng. 34 (1992) 179.
[6] G. Giannetto, R. Monque, R. Galiasso, Catal. Rev.-Sci. Eng. 36 (1994) 271.
[7] L.B. Young, S.A. Butter, W.W. Kaeding, J. Catal. 76 (1982) 418.
[8] N.Y. Chen, W.E. Garwood, F.G. Dwyer, Shape Selective Catalysis in Industrial Applications, Marcel Dekker, New York, 1996.
[9] H. Kitagawa, Y. Sendoda, Y. Ono, J. Catal. 101 (1986) 12.
[10] G.L. Price, V. Kanazirev, J. Catal. 126 (1990) 267.
[11] E.G. Derouane, S.B. Abdul Hamid, I.I. Ivanova, N. Blom, P. Højlund-Nielsen, J. Mol. Catal. 86 (1994) 371.
[12] C.R. Bayense, J.H.C. van Hooff, Appl. Catal. A 79 (1991) 127.
[13] C.R. Bayense, A.J.H.P. van der Pol, J.H.C. van Hooff, Appl. Catal. 72 (1991) 81.
[14] A. Montes, G. Giannetto, Appl. Catal. A 197 (2000) 31.
[15] N.S. Gnep, J.Y. Doyemet, A.M. Seco, F.R. Ribeiro, M. Guisnet, Appl. Catal. 43 (1988) 155.
[16] D. Seddon, Catal. Today 6 (1990) 351.
[17] T. Mole, J.R. Anderson, G. Creer, Appl. Catal. 17 (1985) 127.
[18] L.A. Dufresne, R. Le Van Mao, Catal. Lett. 25 (1994) 371.
[19] H. Berndt, G. Lietz, B. Lucke, J. Volter, Appl. Catal. A 146 (1996) 351.
[20] H. Berndt, G. Lietz, J. Volter, Appl. Catal. A 146 (1996) 365.
[21] T. Inui, F. Okazumi, J. Catal. 90 (1984) 366.
[22] C.W.R. Engelen, J.P. Wolthuizen, J.H.C. van Hooff, Appl. Catal. 19 (1985) 153.
[23] N.S. Gnep, J.Y. Doyemet, A.M. Seco, F.R. Ribeiro, M. Guisnet, Appl. Catal. 35 (1987) 93.
[24] K.H. Steinberg, U. Mroczek, F. Roessner, Appl. Catal. 66 (1990) 37.
[25] B.S. Kwak, W.M.H. Sachtler, W.O. Haag, J. Catal. 149 (1994) 465.
[26] P. Meriaudeau, C. Naccache, Catal. Rev.-Sci. Eng. 39 (1997) 5.
[27] M. Guisnet, N.S. Gnep, D. Aittaleb, Y.J. Doyemet, Appl. Catal. A 87 (1992) 255.
[28] G.A. Olah, Angew. Chem. Int. Ed. 12 (1973) 173.
[29] P. Meriaudeau, G. Sapaly, C. Naccache, J. Mol. Catal. 81 (1993) 293.
[30] J. Bandiera, Y. Bentaarit, Appl. Catal. 62 (1990) 309.
[31] T.F. Narbeshuber, H. Vinek, J.A. Lercher, J. Catal. 157 (1995) 388.
[32] N.S. Gnep, J.Y. Doyement, M. Guisnet, in: H.G. Karge, J. Weitkamp (Eds.), Zeolites as Catalysts, Sorbents and Detergent Builders, Elsevier, Amsterdam, 1989, p. 153.
[33] P. Meriaudeau, C. Naccache, J. Mol. Catal. 50 (1989) L7.
[34] J.N. Miale, P.B. Weisz, J. Catal. 20 (1971) 288.
[35] E. Iglesia, J. Baumgartner, G.L. Price, K.D. Rose, J.L. Robbins, J. Catal. 125 (1990) 95.
[36] D.V. Dass, A.L. Odell, J. Catal. 113 (1988) 259.
[37] Y.V. Joshi, A. Bhan, K.T. Thomson, J. Phys. Chem. B 108 (2004) 971.
[38] V.B. Kazansky, Acc. Chem. Res. 24 (1991) 379.
[39] I.N. Senchenya, V.B. Kazansky, Catal. Lett. 8 (1991) 317.
[40] A. Bhan, Y.V. Joshi, W.N. Delgass, K.T. Thomson, J. Phys. Chem. B 107 (2003) 10476.
[41] M. Boronat, P.M. Viruela, A. Corma, J. Am. Chem. Soc. 126 (2004) 3300.
[42] J.A. Lercher, R.A. van Santen, H. Vinek, Catal. Lett. 27 (1994) 91.
[43] V.B. Kazansky, Catal. Today 51 (1999) 419.
[44] S.A. Zygmunt, L.A. Curtiss, P. Zapol, L.E. Iton, J. Phys. Chem. B 104 (2000) 1944.
[45] A.M. Rigby, G.J. Kramer, R.A. van Santen, J. Catal. 170 (1997) 1.
[46] M.V. Frash, V.B. Kazansky, A.M. Rigby, R.A. van Santen, J. Phys. Chem. B 102 (1998) 2232.
[47] M. Boronat, P. Viruela, A. Corma, J. Phys. Chem. B 101 (1997) 10069.
[48] V.B. Kazansky, M.V. Frash, R.A. van Santen, Catal. Lett. 48 (1997) 61.
[49] S.R. Blaszkowski, M.A.C. Nascimento, R.A. van Santen, J. Phys. Chem. 100 (1996) 3463.
[50] E.A. Furtado, I. Milas, J. Lins, M.A.C. Nascimento, Phys. Status Solidi A 187 (2001) 275.

[51] J.F. Haw, B.R. Richardson, I.S. Oshiro, N.D. Lazo, J.A. Speed, J. Am. Chem. Soc. 111 (1989) 2052.
[52] J. Sauer, M. Sierka, J. Comput. Chem. 21 (2000) 1470.
[53] P. Sherwood, A.H. de Vries, S.J. Collins, S.P. Greatbanks, N.A. Burton, M.A. Vincent, I.H. Hillier, Faraday Discuss. (1997) 79.
[54] H.V. Koningsveld, H.V. Bekkum, J.C. Jansen, Acta Crystallogr. Sect. B: Struct. Sci. B 43 (1987) 127.
[55] K.-P. Schroder, J. Sauer, M. Leslie, C. Richard, A. Catlow, Zeolites 12 (1992) 20.
[56] A.D. Becke, J. Chem. Phys. 98 (1993) 5648.
[57] S. Kasuriya, S. Namuangruk, P. Treesukol, M. Tirtowidjojo, J. Limtrakul, J. Catal. 219 (2003) 320.
[58] G.J. Kramer, R.A. van Santen, J. Am. Chem. Soc. 117 (1995) 1766.
[59] S. Dapprich, I. Komaromi, K.S. Byun, K. Morokuma, M.J. Frisch, J. Mol. Struct. THEOCHEM 462 (1999) 1.
[60] A.K. Rappe, C.J. Casewit, K.S. Colwell, W.A. Goddard, W.M. Skiff, J. Am. Chem. Soc. 114 (1992) 10024.
[61] Gaussian 03, Revision B.5, M.J. Frisch, G.W. Trucks, H.B. Schlegel, G.E. Scuseria, M.A. Robb, J.R. Cheeseman, J. Montgomery, J.A.T. Vreven, K.N. Kudin, J.C. Burant, J.M. Millam, S.S. Iyengar, J. Tomasi, V. Barone, B. Mennucci, M. Cossi, G. Scalmani, N. Rega, G.A. Petersson, H. Nakatsuji, M. Hada, M. Ehara, K. Toyota, R. Fukuda, J. Hasegawa, M. Ishida, T. Nakajima, Y. Honda, O. Kitao, H. Nakai, M. Klene, X. Li, J.E. Knox, H.P. Hratchian, J.B. Cross, C. Adamo, J. Jaramillo, R. Gomperts, R.E. Stratmann, O. Yazyev, A.J. Austin, R. Cammi, C. Pomelli, J.W. Ochterski, P.Y. Ayala, K. Morokuma, G.A. Voth, P. Salvador, J.J. Dannenberg, V.G. Zakrzewski, S. Dapprich, A.D. Daniels, M.C. Strain, O. Farkas, D.K. Malick, A.D. Rabuck, K. Raghavachari, J.B. Foresman, J.V. Ortiz, Q. Cui, A.G. Baboul, S. Clifford, J. Cioslowski, B.B. Stefanov, G. Liu, A. Liashenko, P. Piskorz, I. Komaromi, R.L. Martin, D.J. Fox, T. Keith, M.A. Al-Laham, C.Y. Peng, A. Nanayakkara, M. Challacombe, P.M.W. Gill, B. Johnson, W. Chen, M.W. Wong, C. Gonzalez, J.A. Pople, Gaussian, Inc., Pittsburgh PA, 2003.
[62] M. Sierka, J. Sauer, Faraday Discuss. 106 (2002) 41.
[63] X. Rozanska, T. Demuth, F. Hutschka, J. Hafner, R.A. van Santen, J. Phys. Chem. B 106 (2002) 3248.
[64] J.M. Vollmer, E.V. Stefanovich, T.N. Truong, J. Phys. Chem. B 103 (1999) 9415.
[65] L.A. Clark, M. Sierka, J. Sauer, J. Am. Chem. Soc. 126 (2004) 936.
[66] E.V. Stefanovich, T.N. Truong, J. Phys. Chem. B 102 (1998) 3018.
[67] A.H. de Vries, P. Sherwood, S.J. Collins, A.M. Rigby, M. Rigutto, G.J. Kramer, J. Phys. Chem. B 103 (1999) 6133.
[68] P.E. Sinclair, A. de Vries, P. Sherwood, C.R.A. Catlow, R.A. van Santen, Faraday Transact. 94 (1998) 3401.
[69] M. Brandle, J. Sauer, J. Mol. Catal. A 119 (1997) 19.
[70] M. Sierka, J. Sauer, J. Phys. Chem. B 105 (2001) 1603.
[71] C. Tuma, J. Sauer, Chem. Phys. Lett. 387 (2004) 388.
[72] C.Y. Peng, H.B. Schlegel, Isr. J. Chem. 33 (1993) 449.
[73] C. Gonzalez, H.B. Schlegel, J. Chem. Phys. 90 (1989) 2154.
[74] X. Rozanska, R.A. van Santen, T. Demuth, F. Hutschka, J. Hafner, J. Phys. Chem. B 107 (2003) 1309.
[75] X. Rozanska, R.A. van Santen, F. Hutschka, J. Hafner, J. Am. Chem. Soc. 123 (2001) 7655.
[76] M. Hesse, Ring Enlargement in Organic Chemistry, VCH, Weinheim, 1991.
[77] D.M. Brouwer, J.M. Oelderik, Recl. Trav. Chim. Pays-Bas 87 (1968) 721.
[78] T. Demuth, X. Rozanska, L. Benco, J. Hafner, R.A. van Santen, H. Toulhoat, J. Catal. 214 (2003) 68.
[79] J. March, Advanced Organic Chemistry: Reactions, Mechanisms, and Structure, McGraw-Hill, New York, 1977.